Author/s:
Zeng, J;Shen, JP;Wang, JT;Hu, HW;Zhang, CJ;Bai, R;Zhang, LM;He, JZ

Title:
Impacts of Projected Climate Warming and Wetting on Soil Microbial Communities in Alpine Grassland Ecosystems of the Tibetan Plateau

Date:
2018-05-01

Citation:
Zeng, J., Shen, J. P., Wang, J. T., Hu, H. W., Zhang, C. J., Bai, R., Zhang, L. M. & He, J. Z. (2018). Impacts of Projected Climate Warming and Wetting on Soil Microbial Communities in Alpine Grassland Ecosystems of the Tibetan Plateau. Microbial Ecology, 75 (4), pp.1009-1023. https://doi.org/10.1007/s00248-017-1098-4.

Persistent Link:
https://hdl.handle.net/11343/282980

Impacts of projected climate warming and wetting on soil microbial communities in alpine grassland ecosystems of the Tibetan Plateau

Jun Zeng[1,2,3], Ju-Pei Shen[1*], Jun-Tao Wang[1], Hang-Wei Hu[4], Cui-Jing Zhang[1], Ren Bai[1], Li-Mei Zhang[1,2], Ji-Zheng He [1,2,4*]

[1]State Key Laboratory of Urban and Regional Ecology, Research Center for Eco-Environmental Sciences, Chinese Academy of Sciences, 100085 Beijing, China

[2]College of Resources and Environment, University of the Chinese Academy of Sciences, 100049 Beijing, China

[3]Institute of Applied Microbiology, Xinjiang Academy of Agricultural Sciences, 830091 Urumqi, China

[4]Faculty of Veterinary and Agricultural Sciences, The University of Melbourne, VIC 3010 Parkville, Australia

Corresponding author*:

Ju-Pei Shen or Ji-Zheng He, Phone: +86 10 62849788; E-mail: jpshen@rcees.ac.cn or jizheng.he@unimelb.edu.au

Abstract

Climate change is projected to have impacts on precipitation and temperature regimes in drylands of high elevation regions, with especially large effects in the Qinghai-Tibetan Plateau. However, there was limited information about how the projected climate change will impact on the soil microbial community and their activity in the region. Here, we present results from a study conducted across 72 soil samples from 24 different sites along a temperature and precipitation gradient (substituted by aridity index ranging from 0.079 to 0.89) of the Plateau, to assess how changes in aridity affect the abundance, community composition and diversity of bacteria, ammonia-oxidizers and denitrifers (*nirK*/*S* and *nosZ* genes-containing communities) as well as nitrogen (N) turnover enzyme activities. We found V-shaped or inverted V-shaped relationships between the aridity index (AI) and soil microbial parameters (gene abundance, community structures, microbial diversity, and N turnover enzyme activities) with a threshold at AI=0.27. The increasing or decreasing rates of the microbial parameters were higher in areas with AI<0.27 (alpine steppes) than in mesic areas with 0.27<AI<0.89 (alpine meadow and swamp meadow). The results indicated that the projected warming and wetting have a strong impact on soil microbial communities in the alpine steppes.

Keywords: Climate change; Warming and wetting; Bacterial *16S rRNA*; Nitrification; Denitrification; Alpine grassland

Introduction

Global warming is an indisputable fact, which has caused the increase of

approximately 0.75 ^{o}C in the earth's surface temperature over the last Century [22]. As a consequence of global warming, changes in precipitation patterns, including in the amount, intensity, frequency, and type of precipitation, have already occurred around the world within the past few decades [18]. A continuous and more rapid warming trend during this century has been simulated by many models (*e.g.*, General circulation models, IPCC climate model and so on), which are predicted to increase by 1.8-4.0 ^{o}C [23]. In general, global climate pattern represents more warmer and wetter climate change in the mid- to high latitudes of the Northern Hemisphere.

The warming rate is amplified with elevation, which is particularly true to the Qinghai-Tibetan plateau [31]. As the highest (>4000 m above sea level, a.s.l.) and largest plateau (with a size of about 2.5 million km^2) on earth, the Qinghai-Tibetan plateau is very sensitive to changes in climate, and served as a sensitive indicator of regional and global climate change [42]. During the last 60 years (1951–2012), the plateau experienced a warming at a rate of 0.36 ^{o}C per decade [29, 47], which is threefold the average global rate (0.12 ^{o}C) [23]. The mean annual precipitation trends show a significant increase during the winter and spring since 1960 [29]. The IPCC global climate models clearly indicate that the warming and wetting trend on the Qinghai-Tibetan Plateau will continue, while mean annual temperature and mean annual precipitation are expected to increase by 2.6 - 5.2 ^{o}C and 38 - 272 mm, respectively by 2100 [8, 22, 31, 57].

A growing body of evidence has demonstrated that climate warming and changing precipitation can profoundly influence soil ecosystem processes [6-8, 11, 25,

35]. For instance, elevated temperature can influence the aboveground net primary production and therefore impact the pool and input of available substrates utilized for microbial growth in the underground ecosystem [52]. Elevated temperature can directly impact the soil microbial community abundance, structure, biomass and activity [46]. A result from a global survey of dryland showed that increased aridity with climate change is a major driver of biodiversity loss in terrestrial ecosystems [32]. Altered precipitation regimes caused by elevated temperature also increase the evaporative flux of water from the soil and therefore indirectly affect microorganisms [33, 51]. Soil drying will dramatically alter the functioning of natural ecosystems, such as decoupling of biogeochemical cycles of C, N and P under rapid climate change [9]. Besides, the extreme climate driven soil drying-rewetting cycles could pulse on soil microbial respiration (the ‘‘Birch Effect’’) [3] and N mineralization [34]. These changes may influence the turnover of the soil organic matter (SOM), which plays an important role in the global C cycle and may further intensify the warming at regional and even global scales [53].

However, there is limited information about how the soil microbial communities and their potential to emit greenhouse gases respond to climate change in high elevation regions [37]. Previous studies on the effect of climate change on soil microbial communities in the Plateau were mainly conducted by using artificial warming [62], observational investigations along an elevation gradient [55, 61], and/or garden transplant experiments [30, 63]. However, artificial warming and soil transplant experiments may underestimate the responses of microbial communities to

the climate change [41, 50]. Additionally, artificial simulation of the climate change can only reflect the influence of a particular climate zone on the soil microbial community [59]. To address the question and to better understand how the microbial community might respond to climate change in the alpine ecosystems, we collected soil samples along a strong temperature and precipitation gradient from west to east of the Tibetan Plateau. Due to the temperature and precipitation gradients the corresponding ecosystems are arid, semi-arid and humid, and hence we used the aridity index (AI, where AI is mean annual precipitation/potential evapotranspiration) as a proxy for the parameters of climate change [32, 48, 49]. The gradient covered an aridity gradient with values from AI=0.079 to 0.89, the larger the value, the warmer and wetter itself. We hypothesized that (1) warming and wetting tendency could increase soil microbial community abundance and diversity; (2) warming and wetting could stimulate N cycling functional community-mediated greenhouse gas metabolic ability; (3) microbial communities in the alpine steppes are more sensitive in their response to warming and wetting than microbes in the mesic meadows; (4) there may be a tipping point in the relationship between aridity and soil microbial parameters.

Materials and Methods

Site description and soil sampling

Three predominant grassland ecosystems, including alpine swamp meadow (0.43<AI<0.89), alpine meadow (0.23<AI<0.43) and alpine desert steppe (0.079<AI<0.23) located on the Tibetan Plateau, were selected for the study and their geographical coordinates is summarized in supplementary table s1. The climate of

alpine swamp meadow is a warm temperate damp monsoon, with mean annual temperature (MAT) of 3.2 ^{o}C and mean annual precipitation (MAP) of 700-1100 mm. Soils of alpine swamp meadow are flooded and displayed patchy distributions at the foot of the Sejila Mountain of Nyingchi Prefecture (including LZ-1, LZ-2 and LZ-3). The climate of alpine meadow is a sub-frigid and semi-arid high-plateau monsoon climate, with MAT of -1.2 ^{o}C and MAP of 400 mm. Soils of alpine meadow are very compact and distributed in the Damxung (including MLS, DX, YBJ) and Nagchu (NQ) counties of the northern Tibetan. The climate of alpine desert steppe is a frigid and high-plateau dry climate, with MAT of -4 ^{o}C and MAP of 150 mm. Soils of alpine desert steppe are loosely structured and presented fierce wind erosion and desertification in the north-western of Tibet. A total of 72 soil samples were collected from 24 different sites along the temperature and precipitation gradients of the Plateau (Figure 1). At each sampling site, triplicate samples of the topsoil (0-15 cm) were taken at the vertex of a triangle with an edge distance of 50-100 m in May 2013. Soil samples were collected using a stainless-steel shovel and were mixed uniformly and sealed in plastic bags and shipped to the laboratory.

Soil physicochemical analysis and DNA extraction

The soil samples for physicochemical analysis were air-dried, manually ground, and sieved through a 2-mm mesh to remove large debris, roots and other residue. Soil pH was determined after diluting 3 g of air-dried soil in 7.5 ml of 0.01 M $CaCl_2$ solution and measured by glass electrode using a Mettler Toledo DL-25 pH meter (Shanghai, China, Mettler-Toledo (Shanghai) Ltd). Soil moisture content (SMC) was measured

by oven-drying (Beijing, China, Thermo Scientific (China) Ltd) the samples at 105 ^{o}C for 24 h. Soil cation exchange capacity (CEC) was quantified by extracting exchangeable cations using 1 M neutral ammonium acetate solution. The total nitrogen (TN) and total carbon (TC) contents were determined by dry combustion at 1200 ^{o}C on an LECO CNS 2000 elemental analyzer (Saint Joseph, Indiana, LECO CO.) with infrared and thermal conductivity detectors, respectively. Soil organic carbon (SOC) was determined using the $K_2Cr_2O_7$ oxidation titration method [58] (Thermo Multiskan GO microplate reader, Shanghai, China). Nitrate (NO_3^-–N) and ammonium (NH_4^+–N) were extracted using 2 M KCl at a soil/extractant ratio of 1:5 and measured using a LACHAT Quickchem Automated Ion Analyzer (Loveland, Colorado, Lachet Instruments Loveland, CO.). Climate data were collected from China Meteorological Administration (www.cma.gov.cn)

Soil samples for molecular biology analysis were vacuum freeze-dried, manually ground, sieved through a 2 mm mesh and stored at -80 ^{o}C. DNA was extracted from triplicate soil samples (0.5 g dry soil) using a Power soil DNA isolation kit (MO BIO Laboratories, San Diego, CA, USA) according to the manufacturer's protocol. The quantity of the extracted DNA was checked with NanoDrop ND-2000 UV–vis Spectrophotometers (NanoDrop Technologies, USA).

Quantitative PCR (qPCR) analysis

Quantitative PCR (qPCR) was carried out with a Bio-Rad iQ^{TM} 5 thermocycler (Bio-Rad Laboratories, Hercules, CA, USA) to determine the bacterial and N cycling functional community gene abundance. A TaqMan probe TM1389 was employed to

quantify the bacterial 16S rRNA gene by using the primer pairs 1369 F/1492R, the 3' end of which was marked as TAMRA, whereas the 5' end was marked by FAM [40]. The 25-μl PCR reactions contained 12.5 μl Premix Ex TaqTM (Takara Biotechnology, Dalian, China), 2.5 μM of each primer, 1.5 μM of the Taqman probe, and a 1-μl DNA template (>10 ng). Ammonia-oxidation communities (bacterial and archaeal *amoA* genes) were quantified according to He et al [17]. Denitrifying bacterial abundances (*nirK*/*S* and *nosZ*) were carried out according to Brankatschk et al [2].

Standard curves for real-time PCR assays were developed using primer pairs 27F/1492R (Lane, 1991), amoA1F/amoA2R [39], CrenamoA23f/CrenamoA616r [1], Nirs-cd3aF/Nirs-R3cd [36, 45], nirK-F1aCu/nirK-R3Cu [45] and nosZF/nosZ2R [19] to amplify bacterial *16S rRNA* gene, bacterial *amoA* gene (AOB), archaeal *amoA* gene (AOA), *nirS*, *nirK* and *nosZ* genes from templates, respectively. To get more details on these primer sequences and amplification conditions please see the supplementary table s2. The purified PCR products were ligated into a pMD19-T Vector and transformed into E. Coli JM109 competent cells (TaKaRa, Dalian, China). The transformed cells were plated on Luria-Bertani plates containing 100 μl of ampicillin (100mg·ml^{-1}), 100 μl of IPTG (24 mg·ml^{-1}), 200 μl of X-Gal (50 mg·ml^{-1}) and incubated for 12-16 h at 37 ^{o}C. Plasmids from the positive clone that screened by blue-white spot screening with the target gene insert were extracted for sequencing and used as standards for calibration curves. The plasmid concentration was determined on a Nanodrop ® ND-1000 UV-Vis Spectrophotometer and used for the calculation of standard copy numbers. Ten-fold serial dilutions of a known copy

number of the plasmid were subject to real-time PCR assay in triplicate to generate an external standard curve.

Miseq sequencing analysis of the bacterial 16S rRNA gene amplicons

The primer pair 515 F (5'- GTGCCAGCMGCCGCGG -3') and 907R (5'- CCGTCAATTCMTTTRAGTTT -3') was used to amplify the V4 region of the bacterial *16S rRNA* gene [64]. Primer sequences were modified by adding Illumina adaptor A to the 5′-ends of the forward primers, and adaptor B followed by 12 nucleotide barcode sequences to the 3′-ends of the reverse primers. The 50 μl reaction system consists of 20 μl Premix Ex Taq (Takara Biotechnology, Dalian, China), 0.4 μl of each primer (10 μM), 4 μl of five-fold diluted template DNA (1-10 ng) and 25.2 μl sterilized water. Thermal cycling conditions were an initial denaturation of 3 min at 94 °C; six touch down cycles of 45 s at 94 °C, 60 s from 65 °C to 58 °C, 70 s at 72 °C, followed by 22 cycles of 45 s at 94 °C, 60 s at 58 °C, and 60 s at 72 °C, with a final elongation of 72 °C for 10 min. The PCR products were purified using a Wizard SV Gel and PCR Clean-up system (Promega, USA), and then sequenced on the MiSeq platform (Illumina, San Diego, CA, USA) at Novogene, Beijing, China. High-quality raw sequences were processed using the UPARSE to pick operational taxonomic units (OTUs) at the ≥97 % identity threshold and filter chimera sequences [12]. Representative sequences were processed using the QIIME [5]. PyNAST alignment, and ribosomal database project (RDP) assignment were carried out based on the latest Green genes database 4 (http://greengenes.lbl.gov/). We used a randomly selected subset of 34565 sequences per sample for subsequent community analysis. Sequences

of the bacterial 16S rRNA gene have been deposited in the DNA Data Bank of European Molecular Biology Laboratory (EMBL) under the accession number PRJEB13060.

Terminal restriction fragment length polymorphism (T-RFLP) analysis

The FAM-labeled PCR products were digested with *Rsa* I (AOA), *Hha* I (AOB), and *Hae* III (*nosZ*) in 20 μl reactions. Three replicates of PCR products were mixed at the equal quantity ratio and purified using a Wizard SV Gel and PCR Clean-up system (Promega, San Luis Obispo, CA, USA). The mixture (20 μl) contained 2 μl of 10×Buffer, 0.5 μl of restriction enzyme (10 $U \cdot \mu l^{-1}$, TaKaRa), < 1 μg of amplicon and ddH_2O to adjust the total volume to 20 μl. All the digests were incubated at 37 ^oC for 3 h, followed by deactivation at 95 ^oC for 15 min (supplementary table s2).

Cloning, sequencing and phylogenetic analysis

The purified non-FAM-labeled PCR products (AOA-*amoA*, AOB-*amoA*, *nosZ* genes) were ligated into a pMD19-T Vector and transformed into *E. Coli* JM109 competent cells (TaKaRa, Dalian, China). The transformed cells were plated on Luria-Bertani plates containing 100 μl of ampicillin (100$mg \cdot ml^{-1}$), 100 μl of IPTG (24 $mg \cdot ml^{-1}$), 200 μl of X-Gal (50 $mg \cdot ml^{-1}$) and incubated for 12-16 h at 37 ^oC. In order to identify the T-RFs determined from environmental samples, gene positive clones were re-amplified with their FAM-labeled primer sets and detected according to the above T-RFLP procedure. The positive clones that had the same T-RFs with environmental samples were sequenced by the Sanger sequencing method [66]. The relative abundance of a T-RF was calculated by dividing the peak height of the T-RF by the

total peak height of all T-RFs in the profile. The peaks with heights < 1% of the total peak height were not included for further analyses [4]. FAM-labeled primer sets, PCR reactions, amplification conditions were all listed in the supplementary table s2.

All the functional gene sequences obtained in this study were submitted for comparison to the GenBank databases using the BLAST algorithm. Neighbor-joining phylogenetic trees were constructed from dissimilar distance and pair-wise comparisons with the Jukes–Cantor distance model using the MEGA software (version 6.0) [43]. A bootstrap value of 1000 replications was assessed in the analysis. Each gene sequences obtained from this study has been deposited in the Genbank database under accession numbers: KU937454 to KU937529 (AOA); KU937530 to KU937549 (AOB); KU937550 to KU937627 (*nosZ*).

Enzyme activity assay

Potential nitrification rate (PNR) was performed as a microtiter plate assay following the method described by Hu et al [20]. Briefly, 5 g fresh soil was incubated in 20 ml of 1 mM ammonium sulfate solution amended with 50 ml of 1.5 M sodium chlorate solution. Triplicate samples were incubated at 25 ^{o}C for 24 h in the dark, and nitrite was extracted with 5 ml of 2 M KCl and determined using a spectrophotometer at a wavelength of 540 nm with N-(1-naphthyl) ethylenediamine dihydrochloride [21]. Denitrification enzyme activity (DEA) was determined as reported by Brankatschk et al [2]. Three replicates of 10 g fresh soil were saturated with 0.1 mM glucose and nitrate solution. The headspace of the serum bottle was flushed with helium and 10 % acetylene was added. N_2O was analyzed on a Shimadzu GC-14B (Düsseldorf,

Germany) gas chromatograph. The soil was incubated at 20 ^{o}C and headspace samples were taken after 3 and 6 h. Preliminary experiments showed that in all soils considered, the N_2O production was a linear function of time from 0 to 6 h (data not shown).

Climate data sources

Aridity index (AI, the ratio of precipitation to potential evapotranspiration) [44], MAP and MAT data of each sampling site were obtained from the WorldClim database (http://www.worldclim.org/bioclim).

Statistical analysis

Functional communities' alpha- and beta-diversity was determined using Shannon index (*H'*) and Bray-Curtis index, respectively by QIIME 1.7.0 [5]. Bacterial beta-diversity was determined using weighted UniFrac distance. Spearman's correlation analysis was conducted to examine the relationships between the microbial gene abundances (bacterial *16S rRNA*, *amoA*, *nirS/K* and *nosZ*) and environmental parameters in SPSS 21.0 (IBM Co., Armonk, New York). The significance of the community composition difference was tested by the permutation multivariate analysis of variance (PERMANOVA) in R 3.2.2 using the Vegan package [26]. A Mantel test was performed to examine the relationships between soil physiochemical factors and microbial community compositions.

Structural equation model (SEM) was constructed to investigate the direct and indirect effects of AI and physical/chemical variables on biological variables (gene abundance, composition and diversity) and N turnover activities (nitrification and

denitrification enzyme activities). We devised three distinct full models with bacterial diversity, PNR and DEA, N-cycling functional diversity as dependent variables. Diversity was characterized by Shannon-Weiner index, and composition was characterized by first axis of principal component analysis (PCA) by using Euclidian dissimilarity matrix. Based on the theoretical knowledge, we assumed that the climatic parameters (Aridity index) determined soil physical and chemical parameters and their changes affect the variations of microbial abundance, diversity, composition and N turnover activities. Maximum likelihood estimation method was used to compare the SEM with the observation. Model adequacy was determined by χ^2-tests, Akaike Information Criteria (AIC), goodness-of-fit index (GFI) and root square mean errors of approximation (RMSEA). Adequate model fits were indicated by a non-significant χ^2-test ($P > 0.05$), low AIC and RMSEA (<0.05), but high GFI (>0.90) [14]. Finally, we revised our conceptual model based on these indexes. SEM analysis was performed using IBM SPSS AMOS 21.0 (Amos Development Corporation, Meadville, PA, USA).

Results

Variations of soil physicochemical properties, spatial parameters and climate factors along the aridity gradient

The aridity index (AI) is the ratio between precipitation to potential evapotranspiration, and thus the higher the value the higher the moisture [44]. In this study, AI ranged from 0.079 to 0.89, which was significantly and positively correlated with MAP (r=0.99, p<0.01), MAT (r=0.47, p<0.01) and SMC (r=0.68, p<0.01) from

west to east in the Tibetan plateau (Figure 2). Notably, we found a quadratic relationship between AI and all soil parameters with a threshold at AI= 0.27. Soil TN, TC, CEC, SOC, and C/N ratio significantly increased in the area with AI < 0.27, but most did not significantly change in the area with 0.27<AI<0.89. Soil pH ranging from 4.69 to 8.98 showed a significantly linear decline in the area with AI<0.27 (R^2=0.33, p<0.01), while pH was relatively stable in the area with 0.27<AI<0.89 (R^2=0.028, p>0.05) (Figure 2).

Changes of soil bacterial abundance and structure along the AI gradient

The log normalized bacterial *16S rRNA* gene abundance showed a quadratic relationship between AI, which significantly increased in samples with AI<0.27, but it significantly decreased in areas with 0.27<AI<0.89 (Figure 3A). Spearman correlation analysis showed that soil nutrient (TC, TN and SOC) levels have greatest influences on bacterial abundance, followed by soil pH and spatial parameters (Supplementary table S3).

None-metric multidimensional scaling (NMDS) based on the weighted unifrac dissimilarity matrices showed that the whole bacterial composition was distributed according to the AI=0.27 as a critical value (Figure 3B). Further linear regression between bacterial beta-diversity (NMDS1) and aridity index showed the slopes of soil samples with AI<0.27 were higher than in samples in areas with 0.27<AI<0.89 (Figure 3C). The relative abundance of soil microbial phyla also showed a significant shifting pattern at a threshold of AI=0.27. For example, *Acidobacteria, Actinobacteria, Bacteroidetes* and *Proteobacteria* were the most dominant phyla of the bacterial

community, and the relative abundance of *Acidobacteria* (R^2=0.17, p<0.01), *Bacteroidetes* (R^2=0.20, p<0.01), and *Proteobacteria* (including α-, β-, γ-, and δ-*Proteobacteria*) (p<0.01) significantly increased, whereas *Actinobacteria* (R^2=0.24, p<0.01) and *Chloroflexi* (R^2=0.35, p<0.01) significantly decreased in areas with AI<0.27. The relative abundance of the most prominent bacterial phyla has a stable trend in areas with 0.27<AI<0.89 (Figure 3D). The Mantel test showed all soil parameters were significantly correlated with bacterial community compositions (p<0.01). Of these, AI had the largest influence on soil bacterial communities, followed by MAP and SMC (Supplementary Table S4).

Changes in abundance and structure of the N cycling functional communities along the AI gradient

Nearly all of the standardized N cycling microbial functional gene abundances (except for AOB) significantly increased in samples with AI<0.27, but them (except for *nirS* and *nosZ* genes) significantly decreased in areas with 0.27<AI<0.89 (Figure 4A). Abundances of AOA-*amoA* and AOB-*amoA* were mainly influenced by MAT, but the abundances of denitrifies were highly correlated with soil nutrients (TC, TN, SOC, CEC), pH, MAP and geographic locations (Supplementary table S3).

The N cycling functional communities (AOA, AOB and *nosZ*) were detected by the combination of T-RFLP and clone library approaches. The overall N cycling functional community compositions also presented clear shifting patterns with a threshold at AI= 0.27, which showed linear decreasing patterns in areas with AI<0.27, but were significantly increased (except for AOB) in areas with 0.27<AI<0.89 (Figure

4B). In the AOA community, 7 T-RFs classified into 4 clusters (soil and sediment 1, 2, 3 and *Nitrosotalea* cluster), were detected in all the soil samples (Supplementary Figure S1 and S2). The relative abundance of soil and sediment 1 (T-RFs 61 bp) significantly decreased in areas with AI<0.27, but greatly increased in areas with 0.27<AI<0.89. On the contrary, soil and sediment 2 (T-RFs 19, 202, 324 and 385bp) presented an opposite trend compared with the soil and sediment 1 group (Figure 4C). The AOB community was comprised of 8 clusters (cluster 1, 2R, 7, 9, 3a.1, 3a.2, 3b and cluster ME) (Supplementary Figure S3 and S4). Cluster 3b (T-RF 247 bp, ranging from 12.8 to 55.5%) was the predominant group in the selected soils, which slightly increased along the gradient. Cluster 3a.2 (T-RFs 251 bp) was the dominate group in semi-arid soils, and their fractions decreased in the region, but relatively stable in more mesic soils. In contrast, the relative abundance of cluster 1 (T-RFs 67 bp, ranging from 2.8 to 18.7 %) increased along the AI gradient with a greater increasing rate in areas with AI<0.27 (Figure 4D). T-RFs 116 bp (*Rhodopseudomonas palustris*, CP000250, 91 % of gene similarity), and 44 bp, 55bp (*Chelatococcus sp*, CP012399, 91 % of gene similarity) were the most dominant *nosZ*-containing communities in the selected soils. The relative abundance of *Rhodopseudomonas* significantly increased in areas with AI<0.27, and decreased in areas with 0.27<AI<0.89. In contrast, the relative abundance of *Chelatococcus* significantly decreased in areas with AI<0.27, but relatively stable in areas with 0.27<AI<0.89 (Supplementary Figure S5 and S6, Figure 4E).

Changes in potential nitrification rate (PNR) and denitrification enzyme activity

(DEA) along the AI gradient

PNR decreased from 0.1 to 0.004 nmol NO_2^- h^{-1} g^{-1} in soils with AI<0.27, but slightly increased up to 0.029 nmol NO_2^- h^{-1} g^{-1} in areas with 0.27<AI<0.89. Both AOA (r=0.27, p<0.05) and AOB (r=0.30, p<0.01) abundances were positively correlated to PNR. In contrast, DEA significantly increased with the increase of AI in areas with AI<0.27, but with a greater increase in areas with 0.27<AI<0.89, where activity increased from 0.045 to 32 nmol N_2O h^{-1} g^{-1} (r=0.51, p=0.001). The abundances of *nirK*/*S* (r=0.44, p<0.01 and r=0.36, p<0.01) and *nosZ* (r=0.25, p<0.05) were significantly and positively correlated with DEA (Figure 5). PNR was positively and significantly related to SOC (r=2.7, p<0.01), TN (r=3.3, p<0.01) and TC (r=3.2, p<0.01), whereas it was negatively related to NO_3^- (r=-0.30, p<0.05). Nearly all of the soil parameters (soil pH, SOC, SMC, CEC, clay, sand, NH_4^+, NO_3^-), climate factor (MAP), and longitude were significantly correlated to DEA (Supplementary table s3).

Shift of overall soil microbial alpha-diversity along the AI gradient

The overall alpha-diversity (Shannon-Weiner index) of bacteria, ammonia-oxidizers (AOA and AOB), and denitrifiers (*nosZ*) all showed a clearly changing pattern with a threshold at AI=0.27 (Figure 6). For example, all soil microbial diversity showed a decreasing trend in areas with AI<0.27, but to the contrary, had greatly increased (AOB and *nosZ*-containing microbial diversity) or decreased (bacterial diversity) in areas with 0.27<AI<0.89 (Figure 6). Spearman's correlation analysis showed that CEC (r=-0.53, p<0.001), SMC (r=-0.61, p<0.001), SOC (r=-0.60, p<0.001), TC (r=-0.61, p<0.01) and pH (r=0.41, p<0.01) were significantly correlated with bacterial

diversity. TC (r=0.27, *p*=0.023) and NH_4^+ (r=0.31, *p*=0.009) was positively correlated with *nosZ*-containing bacterial diversity, while only MAT was positively correlated with alpha-diversity of AOB. None of parameters were correlated with diversity of AOA.

Contributions of AI and soil properties to soil microbial abundance, community structure, diversity and soil enzyme activity

The first principal component of a PCA on the soil physical properties (CEC, Clay, Sand, SMC) explained 66% of the total variances, suggesting that it can be a good descriptor of "soil conditions". All models showed reasonable fits as hypothesized and could explain most of the variance in soil microbial abundance, composition and diversity (Figure 7). The model could explain 57.7%, 57.6% and 45.9 % of the variance in bacterial abundance, composition and diversity, respectively (Figure 7A). AI had a strong direct negative effect on bacterial abundance and diversity, but indirectly impacted bacterial composition by a strong effect on soil pH. AI had a direct negative effect on the abundance of the ammonia oxidizers, but strong positive effects on PNR and DEA (Figure 7B). The abundance of denitrifiers was mainly directly affected by the abundance of ammonia-oxidizers, SOC and soil properties. Soil pH had a direct negative effect on AOA community composition, whereas a strong positive effect on the *nosZ* community was found. The AOB community was only negatively affected by the TN content. AI had a strong positive effect on AOB and *nosZ*-containing microbial diversities (Figure 7C). Standardized total effects (direct plus indirect effects) showed that AI had the largest contribution to the

variation in diversity of bacteria and *nosZ*-containing bacteria, abundance of AOA, AOB and *nirS* genes and DEA (Supplementary Figure S7 A-C).

Discussion

Soil microbial communities in alpine steppes appear more sensitive to climate change

In the study, we provide strong evidence that bacteria, N cycling functional communities and soil N transformation enzyme activities in alpine steppes (AI<0.27) would show a more sensitive response to a warming and wetting climate scenario than mesic alpine meadow and swamp meadow (0.27<AI<0.89). Notably, we also found that soil physical and chemical factors (such as SMC, pH, CEC, SOC, TN, TC and C/N) also showed a significant and strong increase in steppes, but less changed in mesic meadows. These findings may suggest the effect of warming and wetting on soil microbial communities in some way alter soil physical and chemical parameters in alpine grassland ecosystems. Our findings were supported by a long-term soil transplant experiment, which showed soil physical and chemical factors (such as CEC, temperature, SOC) and soil microbial communities significantly changed in soils transplanted from lower to higher elevation in alpine meadows of the Tibetan plateau [30]. Yang et al also showed that vegetation and some soil physical and chemical factors (such as soil pH, temperature and NH_4^+) accounted for the majority of microbial community variation along an elevation gradient in alpine meadows of the Tibetan plateau [55]. However, the result was not consistent with previous research that showed N-cycling microbial functional gene abundances (nitrification and denitrification genes) increased along an aridity index with a threshold at AI=0.32 in

Chinese northern temperate steppes [48]. The discrepancy may be attributed to the sensitivity of climate change to higher elevations in the Tibetan plateau [56]. Numerous studies indicated that warming is more prominent at higher elevations [31, 56]. The increased warming leads to increased soil water evaporation, particularly in arid and semi-arid areas of the plateau which are characterized by high radiation and evaporation, but lower precipitation. Therefore, more severe water availability, which is usually considered as the main driving factor of the soil microbial community and activity in arid and semi-arid drylands in the plateau, may lead to a more sensitive response to precipitation [8, 53]. Delgado-Baquerizo et al showed that increased aridity in drylands may lead to the decoupling of C, N and P cycling, suggesting accelerated warming and wetting could eliminate the effect of aridity stress on both ground vegetation and underground biogeochemical cycling processes [9, 24]. This hypothesis is further supported by the Mantel test in the present study (Supplementary table S4), which showed SMC and precipitation were the most important factors influencing soil microbial communities and activity, indicating the microbial and functioning responses to the availability of water are remarkably more obvious and positive in alpine dryland soils.

Warming and wetting climate reduces soil bacterial diversity by the way of decreasing soil pH

A large number of studies have indicated that global warming and wetting is positively correlated with soil bacterial diversity in dryland ecosystems as we hypothesized [32]. However, a recent study in a temperate grassland ecosystem

showed that a quadratic relationship was observed between aridity index and bacterial diversity - that is, larger diversity in semi-arid grassland than in more mesic areas [49]. We found the aridity index had a significant negative linear correlation with bacterial alpha-diversity (R^2=0.29, p<0.01). This contrary finding in bacterial diversity is most likely related to a significant decrease of soil pH. Soil pH decreased from 8.98 to 5.27 with increasing AI, which was positively correlated with bacterial diversity (r=0.41, p<0.001), with negative correlations with nearly all of the most abundant bacterial phyla. Bacterial phyla such as *Acidobacteria* (r=-0.43, p<0.001), *Bacteroidetes* (r=-0.36, p<0.001), *Alphaproteobacteria* (r=-0.30, p<0.001), *Betaproteobacteria* (r=-0.33, p<0.001), and *Deltaproteobacteria* (r=-0.48, p<0.001), were significantly negative correlated with soil pH. Similar results were found in many continental-scale investigations which showed that soil pH was the major determining factor controlling bacterial composition and diversity [13, 15, 27]. Besides, in the study we found soil pH had a direct negative effect on TC and SOC content. While, TC had a direct negative effect on bacterial composition, but SOC was positively correlated with microbial abundances and diversity. (Figure 6A). The results suggested that abruptly decreasing soil pH could significantly alter bacterial communities involved in SOC decomposition leading to increased plant-derived carbon inputs to soils exceeding increases in decomposition [54]. Yue et al investigated the mechanisms by soil transplant to stimulate warming, and results indicated warming significantly reduced microbial gene abundances involved in decomposition of recalcitrant C substrates, and soil pH was significantly positively correlated with functional

diversity [59].

Warming and wetting could directly increase soil PNR, but this positive impact could be offset by decreased soil pH

The impact of warming and wetting climate change on N cycling functional genes (*amoA*, *nirK*/S and *nosZ* genes) and their mediated N transformation enzyme activities (PNR and DEA) were investigated by SEM, and results showed that AI had a direct strong positive effect on PNR and DEA (Figure 7B). However, standardized total effect results showed that AI was marginally negatively correlated with PNR, but soil pH had a larger and positive effect on PNR (Supplementary Figure S7 B). This may suggest that warming and wetting could directly increase soil potential nitrification activity, but its positive impacts could be indirectly offset by the decreased soil pH. Similar studies have demonstrated that the increase in pH could stimulate gross and net nitrification rates while soil acidification decreased gross and net nitrification rates in forest and grassland soils [8, 21]. Besides, in the N-cycling model we found that the total effect of AOA gene abundance on PNR was larger than AOB gene and AI, suggesting AOA maybe more prominent than AOB in the nitrification process (Supplementary Figure S7 B). This observation was in contrast to previous findings highlighting that nitrification was driven by AOB rather than AOA in nitrogen-rich grassland soils [10]. Several studies have demonstrated that AOA may play the dominant role in acid soil nitrification [16, 20, 60]. Because pH could significantly affect soil ammonia availability that leads to niche specialisation and differentiation between soil AOA and AOB [20, 38]. We found that soil pH had a direct positive

impact on both AOA community compositions but an indirect effect on AOB by affecting TN, suggesting the direct or indirect pH-associated influences might result in the observed changes of ammonia oxidizers in alpine grassland ecosystems. The dominant AOA lineage soil and sediment 1 cluster was negatively correlated (r=-0.25, *p*=0.032) with soil pH. *Nitrosospira* lineage (including 3a.2 and 3b) was predominantly distributed in neutral and alkaline soils, which was the most dominant AOB and significantly related to soil pH.

Warming and wetting climate would promote soil N loss in the mesic alpine meadow

Standardized total effects showed that AI had a strong positive direct effect on DEA, suggesting warming and wetting are probably able to increase N_2O release rates in alpine grassland soil (Supplementary Figure S7 B). The results were in agreement with previous research that showed soil temperature and soil water content (or precipitation) could increase N_2O emissions [8, 25, 61, 65] in alpine meadows on the Qinghai–Tibetan Plateau. Our models also showed that AI indirectly reduces the soil TN content by strongly affecting soil pH, which further supported our hypothesis that warming and wetting could probably reduce the concentration of soil N by way of stimulating N_2O release into the atmosphere. Notably, in the study we found denitrification enzyme activity only slightly increased in areas with AI<0.27, but greatly increased in areas with 0.27<AI<0.89. In contrast, the relative abundance of denitrification marker genes all significantly increased in areas with AI<0.27, whereas only *nirS* gene abundance greatly increased, while other genes (*nosZ* gene) did not respond or decreased (*nirK* gene) in areas with 0.27<AI<0.89. There are two ways to

explain the inconsistency of denitrification enzyme activity and the corresponding abundance of functional genes. Firstly, warming and wetting could significantly stimulate the growth of *nirS*/K and *nosZ* gene-containing communities in water-deficit environments, but their mediated enzyme activities are usually determined by some soil characters (such as water content, organic C, anaerobic condition and NO_3^--N content) [20-21, 38]. Steppe soils, as opposed to mesic soils, are characterized by coarse texture, good aeration and lack of water, which militates against the formation of anaerobic conditions for denitrification. Secondly, enzyme activity and gene abundances merely reflected the genetic potential of denitrification capacity and the potential of microbial participation, such parameters do note denote functional community activity and function [2]. Lennon and Jones argued that a large fraction of the microorganisms in soils were in the dormant state that exhibited metabolical inactivity at some aridity threshold in dryland ecosystems [28]. In addition, the abundance of ammonia oxidizers and PNR all showed a decreasing trend with increasing AI, which correlated significantly with abundances of denitrifers. Synthesizing the above results, we believed that the effect of warming and wetting on N loss may be only marginal in areas with AI<0.27 (alpine steppes), while the mesic regions would likely face a pronounced increase of N_2O release [8, 11, 21, 62].

Conclusion

Soil microbial abundance, community structures, and enzyme activities were presented a clear quadratic relationship with increasing AI and with a consistently threshold value of AI=0.27 in the Qinghai–Tibetan Plateau grassland ecosystems,

indicating a different response mechanism of grassland to climate change. Warming and wetting could significantly increase bacterial and N-cycling microbial functional gene abundance in the alpine steppes but significantly decrease that in more mesic meadows. Soil microbial communities in alpine steppes may be more sensitive to the climate change than in more mesic meadows. Warming and wetting may be contributed to soil C sequestration in alpine steppes through altering soil physical properties and decreasing soil pH. In contrast, N loss caused by warming and wetting could be more obvious in mesic alpine meadows ($0.27<AI<0.89$). In general, we highlight if future climate change increased aridity over the threshold, the responses of microbes and their mediated biogeochemical processes may have profound impacts on soil nutrient cycling, ecosystem stability and services in the most sensitive and fragile ecosystems.

Acknowledgements

This work was financially supported by grants from the National Science Foundation of China (41230857) and the Ministry of Science and Technology of China (2013CB956300). We are grateful to Professor Fan Liu from Huazhong Agricultural University for his assistance in soil sampling and Professor PM Chalk from The University of Melbourne for his valuable comments on this manuscript.

References

1. Avrahami S, Conrad R (2003) Patterns of community change among ammonia oxidizers in meadow soils upon long-term incubation at different temperatures. Appl Environ Microbiol 69: 6152-6164

2. Brankatschk R, Töwe S, Kleineidam K, Schloter M, Zeyer J (2011) Abundances and potential activities of nitrogen cycling microbial communities along a chronosequence of a glacier forefield. ISME J 5: 1025-1037
3. Birch HF (1958) The effect of soil drying on humus decomposition and nitrogen availability. Plant soil 10: 9-31
4. Cao P, Zhang LM, Shen JP, Zheng YM, Di HJ, He JZ (2012) Distribution and diversity of archaeal communities in selected Chinese soils. FEMS Microbiol Ecol 80: 146-158
5. Caporaso JG, Kuczynski J, Stombaugh J et al (2010) QIIME allows analysis of high-throughput community sequencing data. Nat Methods 7: 335-336
6. Chen B, Liu S, Ge J, Chu J (2010) Annual and seasonal variations of Q_{10} soil respiration in the sub-alpine forests of the Eastern Qinghai-Tibet Plateau, China. Soil Biol Biochem 42: 1735-1742
7. Chen H, Wu N, Wang Y et al (2013) Inter-annual variations of methane emission from an open fen on the Qinghai-Tibetan Plateau: a three-year study. PLoS One 8: e53878
8. Chen H, Zhu Q, Peng C et al (2013) The impacts of climate change and human activities on biogeochemical cycles on the Qinghai-Tibetan Plateau. Global Change Biol 19: 2940-2955
9. Delgado-Baquerizo M, Maestre FT, Gallardo A et al (2013) Decoupling of soil nutrient cycles as a function of aridity in global drylands. Nature 502: 672-676
10. Di H, Cameron K, Shen JP, Winefield C, O'callaghan M, Bowatte S, He J (2009)

Nitrification driven by bacteria and not archaea in nitrogen-rich grassland soils. Nat Geosci 2: 621-624

11. Du Y, Cui Y, Xu X, Liang D, Long R, Cao G (2008) Nitrous oxide emissions from two alpine meadows in the Qinghai–Tibetan Plateau. Plant Soil 311: 245-254
12. Edgar RC (2013) UPARSE: highly accurate OTU sequences from microbial amplicon reads. Nat Methods 10: 996-998
13. Fierer N, Jackson RB (2006) The diversity and biogeography of soil bacterial communities. Proc Natl Acad Sci USA 103: 626-631
14. Grace JB (2006) Structural Equation Modeling and Natural Systems Cambridge; NewYork: Cambridge University Press
15. Griffiths RI, Thomson BC, James P, Bell T, Bailey M, Whiteley AS (2011) The bacterial biogeography of British soils. Environ Microbiol 13: 1642-1654
16. Gubry-Rangin C, Hai B, Quince C et al (2011) Niche specialization of terrestrial archaeal ammonia oxidizers. Proc Natl Acad Sci USA 108: 21206-21211
17. He JZ, Shen JP, Zhang LM, Zhu YG, Zheng YM, Xu MG, Di H (2007) Quantitative analyses of the abundance and composition of ammonia-oxidizing bacteria and ammonia-oxidizing archaea of a Chinese upland red soil under long-term fertilization practices. Environ Microbiol 9: 2364-2374
18. Heisler JL, Weltzin JF (2006) Variability matters: towards a perspective on the influence of precipitation on terrestrial ecosystems. New Phytol 172: 189-192
19. Henry S, Bru D, Stres B, Philippot L (2006) Quantitative detection of the *nosZ*

gene, encoding nitrous oxide reductase, and comparison of the abundances of 16S rRNA, *narG*, *nirK*, and *nosZ* genes in soils. Appl Environ Microbiol 72: 5181-5189

20. Hu HW, Zhang LM, Yuan CL, Zheng Y, Wang JT, Chen D, He JZ (2015) The large-scale distribution of ammonia oxidizers in paddy soils is driven by soil pH, geographic distance, and climatic factors. Front Microbiol 6: 938
21. Hu HW, Macdonald CA, Trivedi P, Holmes B, Bodrossy L, He JZ, Singh BK (2015) Water addition regulates the metabolic activity of ammonia oxidizers responding to environmental perturbations in dry subhumid ecosystems. Environ Microbiol 17: 444-461
22. IPCC (2007) Summary for policymakers In: *Climate Change 2007: Impacts, Adaptation and Vulnerability Contribution of Working Group II to the Fourth Assessment Report of the Intergovernmental Panel on Climate Change* (eds Parry ML, Canziani OF, Palutikof JP, Van der Linden PJ, Hanson CE), PP 81–82 Cambridge University Press, Cambridge
23. IPCC (2013) Summary for policymakers In: *Climate Change 2013: The Physical Science Basis Contribution of Working Group I to the Fifth Assessment Report of the Intergovernmental Panel on Climate Change* (eds Stocker TF, Qin D, Plattner GK, Tignor M, Allen SK, Boschung J, Nauels A, Xia Y, Bex V, Midgley PM), PP 1535 Cambridge University Press, Cambridge
24. Jankju-Borzelabad M, Naseri K (2013) Decoupling of soil nutrient cycles as a function of aridity in global drylands. Nature 502: 672

25. Jiang C, Yu G, Fang H, Cao G, Li Y (2010) Short-term effect of increasing nitrogen deposition on CO_2, CH_4 and N_2O fluxes in an alpine meadow on the Qinghai-Tibetan Plateau, China. Atmos Environ 44: 2920-2926
26. Jimenez MA, Jaksic FM, Armesto JJ, Gaxiola A, Meserve PL, Kelt DA, Gutierrez JR (2011) Extreme climatic events change the dynamics and invasibility of semi-arid annual plant communities. Ecol Lett 14: 1227-1235
27. Lauber CL, Hamady M, Knight R, Fierer N (2009) Pyrosequencing-based assessment of soil pH as a predictor of soil bacterial community structure at the continental scale. Appl Environ Microbiol 75: 5111-5120
28. Lennon JT, Jones SE (2011) Microbial seed banks: the ecological and evolutionary implications of dormancy. Nat Rev Microbiol 9: 119-130
29. Li L, Yang S, Wang Z, Zhu X, Tang H (2010) Evidence of warming and wetting climate over the Qinghai-Tibet Plateau. Arct Antarct Alp Res 42: 449-457
30. Liang Y, Jiang Y, WangF et al (2015) Long-term soil transplant simulating climate change with latitude significantly alters microbial temporal turnover. ISME J 9: 2561-2572
31. Liu X, Cheng Z, Yan L, Yin ZY (2009) Elevation dependency of recent and future minimum surface air temperature trends in the Tibetan Plateau and its surroundings. Global Planet Change 68: 164-174
32. Maestre FT, Delgado-Baquerizo M, Jeffries TC et al (2015) Increasing aridity reduces soil microbial diversity and abundance in global drylands. Proc Natl Acad Sci USA 112: 15684-15689

33. Manzoni S, Schimel JP, Porporato A (2012) Responses of soil microbial communities to water stress: results from a meta-analysis. Ecology 93: 930-938
34. Mikha MM, Rice CW, Milliken GA (2005) Carbon and nitrogen mineralization as affected by drying and wetting cycles. Soil Biol Biochem 37: 339–347
35. Melillo JM, Steudler P, Aber JD et al (2002) Soil warming and carbon-cycle feedbacks to the climate system. Science 298: 2173-2176
36. Michotey V, Méjean V, Bonin P (2000) Comparison of methods for quantification of cytochrome cd 1-denitrifying bacteria in environmental marine samples. Appl Environ Microbiol 66: 1564-1571
37. Nie M, Pendall E, Bell C, Gasch CK, Raut S, Tamang S, Wallenstein MD (2013) Positive climate feedbacks of soil microbial communities in a semi-arid grassland. Ecol Lett 16: 234-241
38. Prosser JI, Nicol GW (2012) Archaeal and bacterial ammonia-oxidisers in soil: the quest for niche specialisation and differentiation. Trends Microbiol 20: 523-531
39. Rotthauwe JH, Witzel KP, Liesack W (1997) The ammonia monooxygenase structural gene *amoA* as a functional marker: molecular fine-scale analysis of natural ammonia-oxidizing populations. Appl Environ Microbiol 63: 4704-4712
40. Suzuki MT, Taylor LT, Delong EF (2000) Quantitative analysis of small-subunit rRNA genes in mixed microbial populations via 5′-nuclease assays. Appl Environ Microbiol 66: 4605-4614
41. Sundqvist MK, Sanders NJ, Wardle DA (2013) Community and Ecosystem

Responses to Elevational Gradients: Processes, Mechanisms, and Insights for Global Change. Annual Rev Ecol Evol S 44: 261-280

42. Tang M, Li C, Zhang J (1986) The climate change of Qinghai-Xizang plateau and its neighborhood. Plateau Meteorol 1: 39-49
43. Tamura K, Stecher G, Peterson D, Filipski A, Kumar S (2013) MEGA6: molecular evolutionary genetics analysis version 6. Mol Biol Evol 30: 2725-2729
44. Trabucco A, Zomer RJ (2009) Global Aridity Index (global-aridity) and global potential evapo-transpiration (global-PET) geospatial database CGIAR Consortium for Spatial Information. The CGIAR-CSI GeoPortal Available at wwwcgiar-csiorg/data/globalaridity-and-pet-database
45. Throbäck IN, Enwall K, Jarvis Å, Hallin S (2004) Reassessing PCR primers targeting *nirS*, *nirK* and *nosZ* genes for community surveys of denitrifying bacteria with DGGE. FEMS Microbiol Ecol 49: 401–417
46. Von-Lützow M, Kögel-Knabner I (2009) Temperature sensitivity of soil organic matter decomposition—what do we know? Biol Fert Soils 46: 1-15
47. Wang B, Bao Q, Hoskins B, Wu G, Liu Y (2008) Tibetan Plateau warming and precipitation changes in East Asia. Geophys Res Lett 35: L14702
48. Wang C, Wang X, Liu D et al (2014) Aridity threshold in controlling ecosystem nitrogen cycling in arid and semi-arid grasslands. Nat Commun 5: 4799
49. Wang X, Van-Nostrand JD, Deng Y, LüX, Wang C, Zhou J, Han X (2015) Scale-dependent effects of climate and geographic distance on bacterial diversity patterns across northern China's grasslands. FEMS Microbiol Ecol 91: fiv133

50. Wolkovich EM, Cook B, Allen JM et al (2012) Warming experiments underpredict plant phenological responses to climate change. Nature 485: 494-497
51. Xiang SR, Doyle A, Holden PA, Schimel JP (2008) Drying and rewetting effects on C and N mineralization and microbial activity in surface and subsurface California grassland soils. Soil Biol Biochem 40: 2281-2289
52. Yang YH, Fang JY, Tang YH, Ji CJ, Zheng CY, He JS, Zhu B (2008) Storage, patterns and controls of soil organic carbon in the Tibetan grasslands. Global Change Biol 14: 1592-1599
53. Yang Y, Fang J, Fay PA, Bell JE, Ji C (2010) Rain use efficiency across a precipitation gradient on the Tibetan Plateau. Geophys Res Lett 37: L15702
54. Yang Y, Fang J, Smith P et al (2009) Changes in topsoil carbon stock in the Tibetan grasslands between the 1980s and 2004. Global Change Biol 15: 2723-2729
55. Yang Y, Gao Y, Wang S et al (2014) The microbial gene diversity along an elevation gradient of the Tibetan grassland. ISME J 8: 430-440
56. Yao T, Liu X, Wang N, Shi Y (2000) Amplitude of climatic changes in Qinghai-Tibetan Plateau. Chinese Sci Bull 45: 1236-1243
57. Yao T, Pu J, Lu A, Wang Y, Yu W (2007) Recent glacial retreat and its impact on hydrological processes on the Tibetan Plateau, China, and surrounding regions. Arct Antarct Alp Res 39: 642-650
58. Yeomans JC, Bremner JM (1988) A rapid and precise method for routine

determination of organic carbon in soil. Commun Soil Sci Plan 19: 1467-1476

59. Yue H, Wang M, Wang S et al (2015) The microbe-mediated mechanisms affecting topsoil carbon stock in Tibetan grasslands. ISME J 9: 2012-2020
60. Zhang LM, Hu HW, Shen JP, He JZ (2012) Ammonia-oxidizing archaea have more important role than ammonia-oxidizing bacteria in ammonia oxidation of strongly acidic soils. ISME J 6: 1032-1045
61. Zhang S, Chen D, Sun D, Wang X, Smith JL, Du G (2012) Impacts of altitude and position on the rates of soil nitrogen mineralization and nitrification in alpine meadows on the eastern Qinghai–Tibetan Plateau, China. Biol Fert Soils 48: 393-400
62. Zhang W, Parker K, Luo Y, Wan S, Wallace L, Hu S (2005) Soil microbial responses to experimental warming and clipping in a tallgrass prairie. Global Change Biol 11: 266-277
63. Zhao M, Xue K, Wang F et al (2014) Microbial mediation of biogeochemical cycles revealed by simulation of global changes with soil transplant and cropping. ISME J 8: 2045-2055
64. Zhou J, Wu L, Deng Y et al (2011) Reproducibility and quantitation of amplicon sequencing-based detection. ISME J 5: 1303-1313
65. Zaady E, Groffman PM, Standing D, Shachak M (2013) High N_2O emissions in dry ecosystems. Eur J Soil Biol 59: 1-7
66. Zeng J, Lou K, Zhang CJ et al (2016) Primary Succession of Nitrogen Cycling Microbial Communities Along the Deglaciated Forelands of Tianshan Mountain,

China. Front Microbiol **7**: 1353

Figure legends

Figure 1. Study area and sampling sites. A total of 72 samples from 24 sites along the temperature and precipitation gradients of Tibetan Plateau. Black triangle means sampling sites: LZ: Nyingchi; MLS: Mila Mountain; YBJ: Yambajan; DX: Damxung; NQ: Nagchu; NMC: Namco; BG: Bangor; NM: Nima; GZ: Gerze; CQ: Cuoqin; SG: Saga; DR: Tingri; RKZ: Shigatse

Figure 2. Variations of soil physical and chemical parameters along an aridity gradient. All the parameters showed a similar pattern with increasing AI above and below the threshold AI=0.27. The triangle represents the soil samples in areas with AI<0.27 (60 samples from 20 sites); The circle represents the soil samples in areas with 0.27<AI<0.89 (12 samples from 4 sites). The proportion of variance explained (R^2) of regressions and significant level was tested by spearman correlation analysis.

Figure 3. Changes of bacterial 16S rRNA gene abundance, distributional pattern and the relative abundances of the most dominant lineages of bacteria with increasing aridity index. (A) Correlations between the log normalized bacterial 16S rRNA gene abundances and aridity index. (B) Nonmetric multidimensional scaling (NMDS) plots derived from the weighted unifrac dissimilarity matrices between soils with symbols colored by different aridity index categories for bacteria. (C) Linear regressions between bacterial beta-diversity (NMDS1) and aridity index. (D) Relationships between aridity index and the relative abundance of the most dominant soil bacteria.

The triangle represents the soil samples in areas with AI<0.27; The circle represent the soil samples in areas with 0.27<AI<0.89. The proportion of variance explained (R^2) of regressions and significant level was tested by spearman correlation analysis.

Figure 4. Changes of N cycling microbial functional gene abundances, distributional pattern and the relative abundances of the most dominant lineages of N cycling microbial communities with increasing aridity index. (A) Correlations between the log normalized N cycling microbial functional gene abundances and aridity index. (B) Linear regressions between AOA, AOB and *nosZ*-containing bacterial beta-diversity (NMDS1) and aridity index. (C-E) Relationships between aridity index and the relative abundance of the most dominant AOA (C), AOB (D) and *nosZ*-containing bacteria (E). The triangle represents the soil samples in areas with AI<0.27 (60 samples from 20 sites); The circle represents the soil samples in areas with 0.27<AI<0.89 (12 samples from 4 sites). The proportion of variance explained (R^2) of regressions and significant level was tested by spearman correlation analysis.

Figure 5. Correlations between N turnover enzyme activities and aridity index. (A) Potential nitrification rate; (B) Denitrification enzyme activity.

Figure 6. Changes of microbial alpha-diversity with increasing aridity index. (A) Correlations between bacterial alpha-diversity and aridity index. (B) Correlations between alpha-diversity of AOA and aridity index. (C) Correlations between alpha-diversity of AOB and aridity index. (D) Correlations between *nosZ*-containing bacterial alpha-diversity and aridity index.

Figure 7. Final “Aridity index effects” structural equation modeling results. (A) SEM

fitted to bacterial abundance, composition and diversity; (B) SEM of the aridity index impact on N cycling functional gene abundances and N turnover enzyme activities; (C) SEM of the aridity index impact on N cycling functional community composition and diversity.

Figure 1

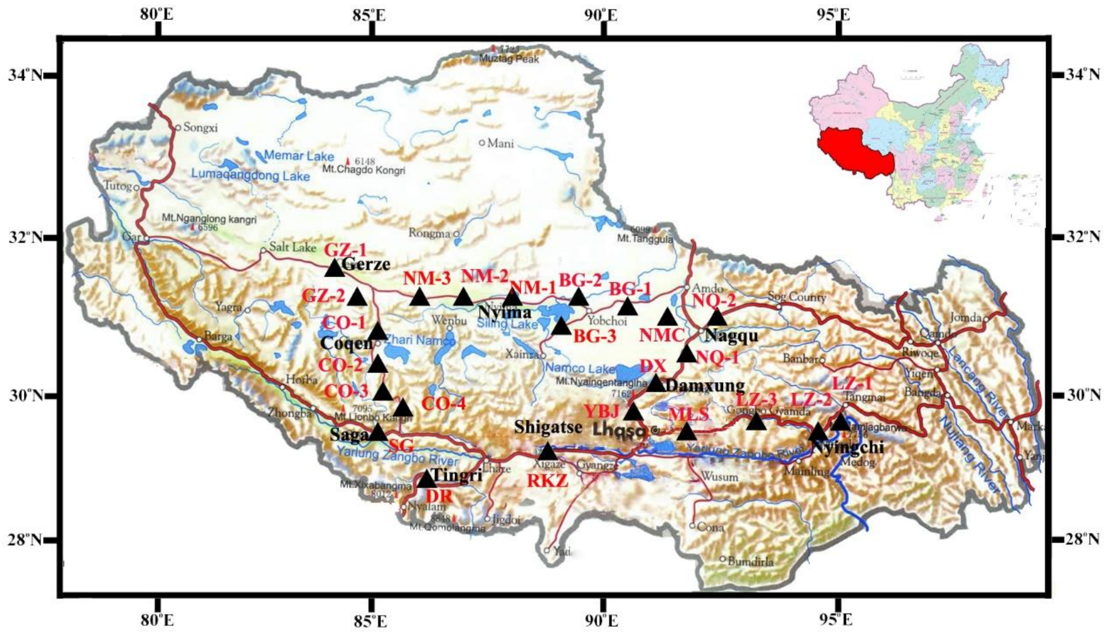

80°E
85°E
90°E
95°E
34°N
32°N
30°N
28°N
GZ-1
Gerze
GZ-2
CO-1
Coqen
CO-2
CO-3
CO-4
Saga
SG
Tingri
DR
NM-3
NM-2
NM-1
Nyima
BG-2
BG-1
BG-3
NMC
NQ-2
Nagqu
NQ-1
DX
Damxung
YBJ
Lhasa
MLS
Shigatse
RKZ
LZ-3
LZ-2
LZ-1
Nyingchi

Figure 2

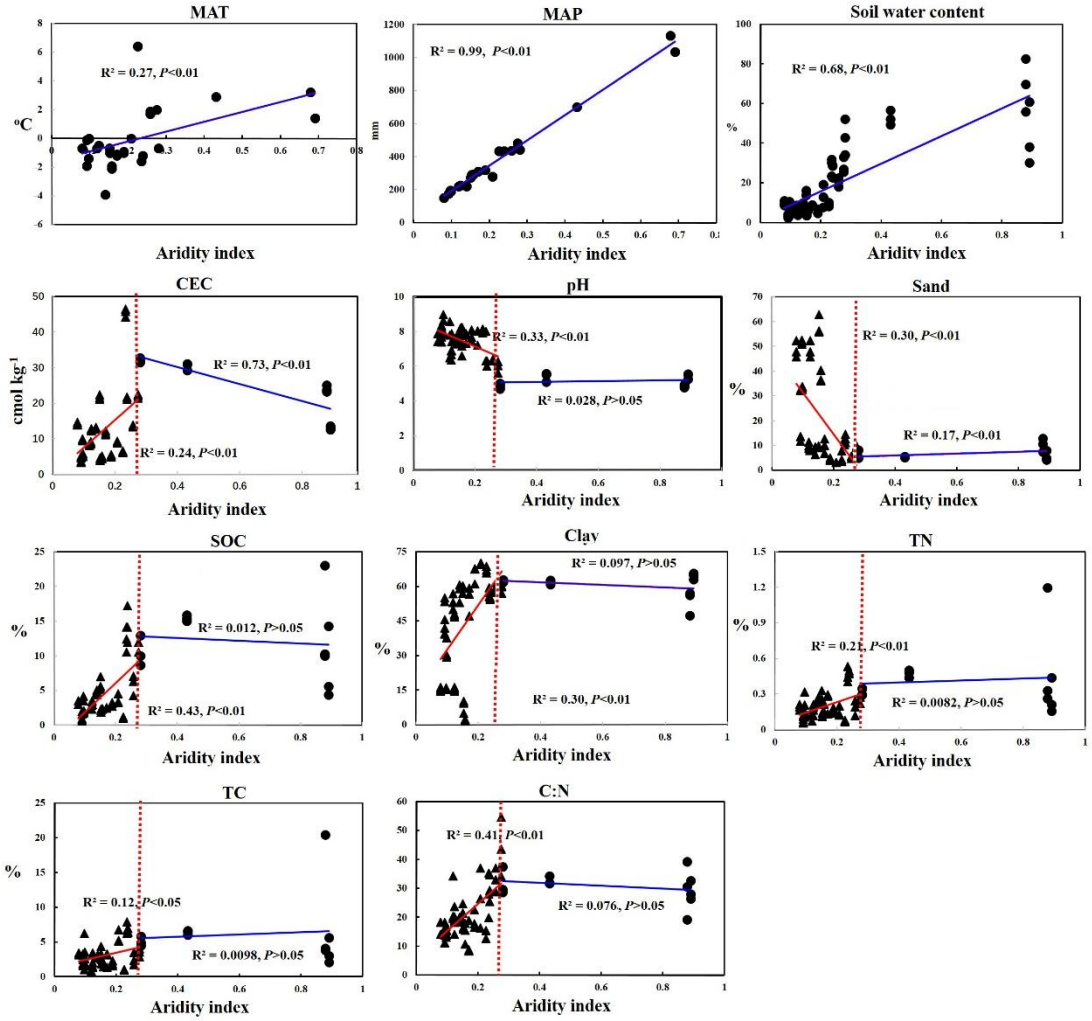
MAT
R² = 0.27, P<0.01
°C
Aridity index
MAP
R² = 0.99, P<0.01
mm
Aridity index
Soil water content
R² = 0.68, P<0.01
%
Aridity index
CEC
R² = 0.73, P<0.01
R² = 0.24, P<0.01
cmol kg-1
Aridity index
pH
R² = 0.33, P<0.01
R² = 0.028, P>0.05
Aridity index
Sand
R² = 0.30, P<0.01
R² = 0.17, P<0.01
%
Aridity index
SOC
R² = 0.012, P>0.05
R² = 0.43, P<0.01
%
Aridity index
Clay
R² = 0.097, P>0.05
R² = 0.30, P<0.01
%
Aridity index
TN
R² = 0.21, P<0.01
R² = 0.0082, P>0.05
%
Aridity index
TC
R² = 0.12, P<0.05
R² = 0.0098, P>0.05
%
Aridity index
C:N
R² = 0.41, P<0.01
R² = 0.076, P>0.05
Aridity index

Figure 3

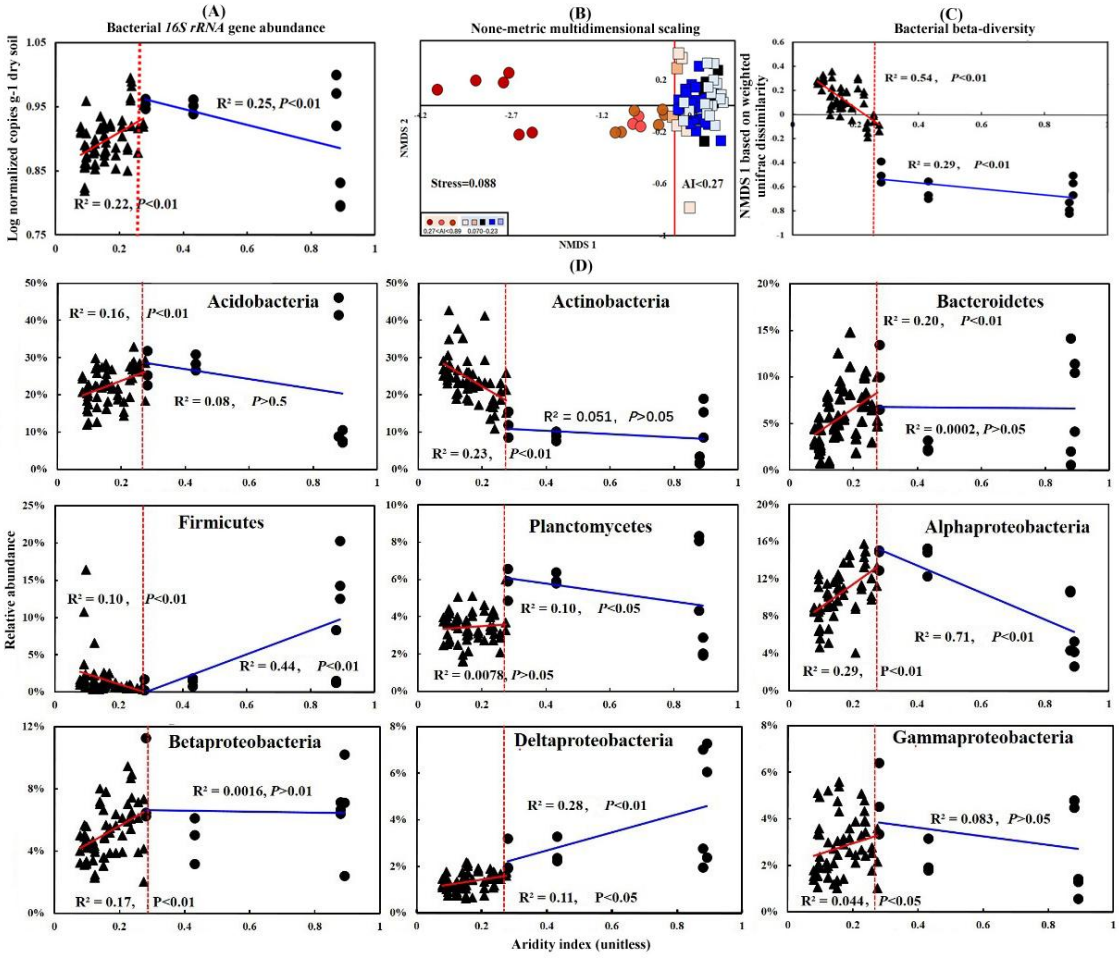
(A)
Bacterial 16S rRNA gene abundance
Log normalized copies g-1 dry soil
R² = 0.25, P<0.01
R² = 0.22, P<0.01
(B)
None-metric multidimensional scaling
NMDS 2
NMDS 1
Stress=0.088
AI<0.27
(C)
Bacterial beta-diversity
NMDS 1 based on weighted unifrac dissimilarity
R² = 0.54, P<0.01
R² = 0.29, P<0.01
(D)
Acidobacteria
R² = 0.16, P<0.01
R² = 0.08, P>0.5
Actinobacteria
R² = 0.051, P>0.05
R² = 0.23, P<0.01
Bacteroidetes
R² = 0.20, P<0.01
R² = 0.0002, P>0.05
Firmicutes
R² = 0.10, P<0.01
R² = 0.44, P<0.01
Planctomycetes
R² = 0.10, P<0.05
R² = 0.0078, P>0.05
Alphaproteobacteria
R² = 0.71, P<0.01
R² = 0.29, P<0.01
Betaproteobacteria
R² = 0.0016, P>0.01
R² = 0.17, P<0.01
Deltaproteobacteria
R² = 0.28, P<0.01
R² = 0.11, P<0.05
Gammaproteobacteria
R² = 0.083, P>0.05
R² = 0.044, P<0.05
Relative abundance
Aridity index (unitless)

Figure 4

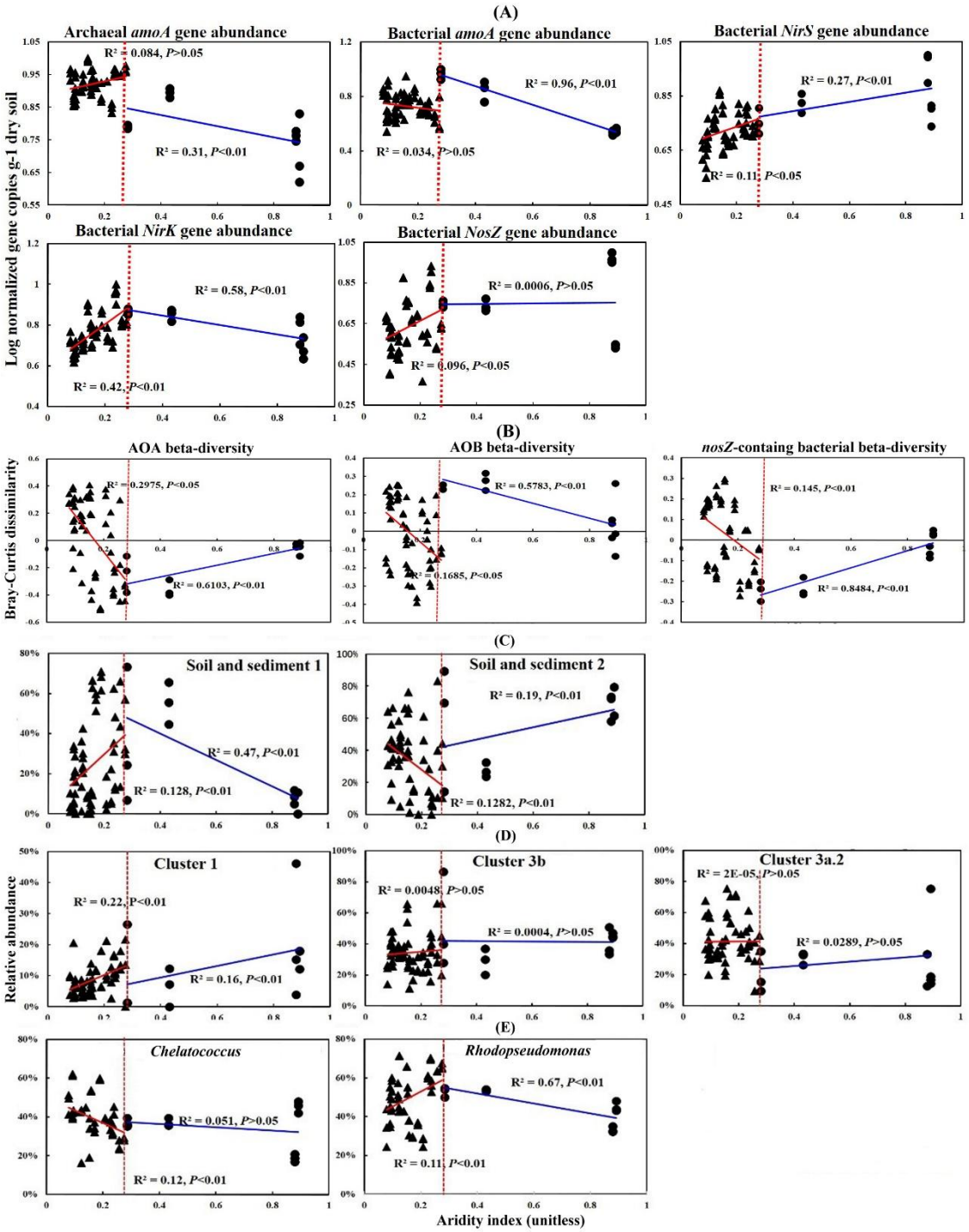
(A)
Archaeal amoA gene abundance
R² = 0.084, P>0.05
R² = 0.31, P<0.01
Bacterial amoA gene abundance
R² = 0.96, P<0.01
R² = 0.034, P>0.05
Bacterial NirS gene abundance
R² = 0.27, P<0.01
R² = 0.11, P<0.05
Bacterial NirK gene abundance
R² = 0.58, P<0.01
R² = 0.42, P<0.01
Bacterial NosZ gene abundance
R² = 0.0006, P>0.05
R² = 0.096, P<0.05
Log normalized gene copies g-1 dry soil
(B)
AOA beta-diversity
R² = 0.2975, P<0.05
R² = 0.6103, P<0.01
AOB beta-diversity
R² = 0.5783, P<0.01
R² = 0.1685, P<0.05
nosZ-containg bacterial beta-diversity
R² = 0.145, P<0.01
R² = 0.8484, P<0.01
Bray-Curtis dissimilarity
(C)
Soil and sediment 1
R² = 0.47, P<0.01
R² = 0.128, P<0.01
Soil and sediment 2
R² = 0.19, P<0.01
R² = 0.1282, P<0.01
(D)
Cluster 1
R² = 0.22, P<0.01
R² = 0.16, P<0.01
Cluster 3b
R² = 0.0048, P>0.05
R² = 0.0004, P>0.05
Cluster 3a.2
R² = 2E-05, P>0.05
R² = 0.0289, P>0.05
Relative abundance
(E)
Chelatococcus
R² = 0.051, P>0.05
R² = 0.12, P<0.01
Rhodopseudomonas
R² = 0.67, P<0.01
R² = 0.11, P<0.01
Aridity index (unitless)

Figure 5

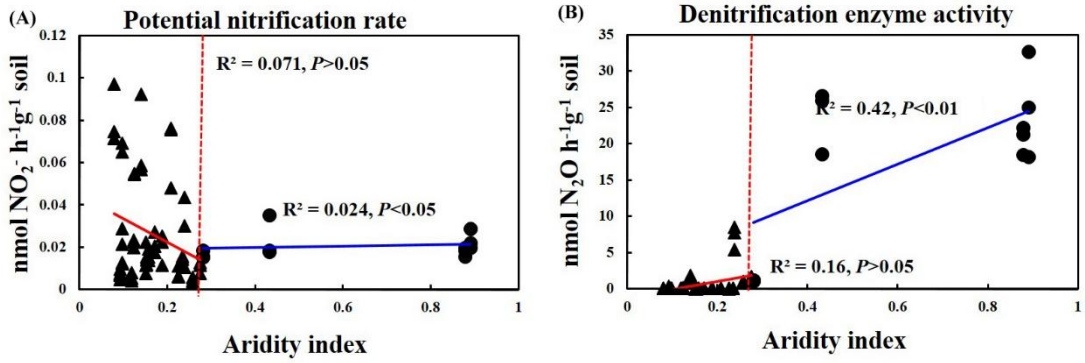
(A)
Potential nitrification rate
nmol NO_2^- $h^{-1}g^{-1}$ soil
R^2 = 0.071, P>0.05
R^2 = 0.024, P<0.05
Aridity index
(B)
Denitrification enzyme activity
nmol N_2O $h^{-1}g^{-1}$ soil
R^2 = 0.42, P<0.01
R^2 = 0.16, P>0.05
Aridity index

Figure 6

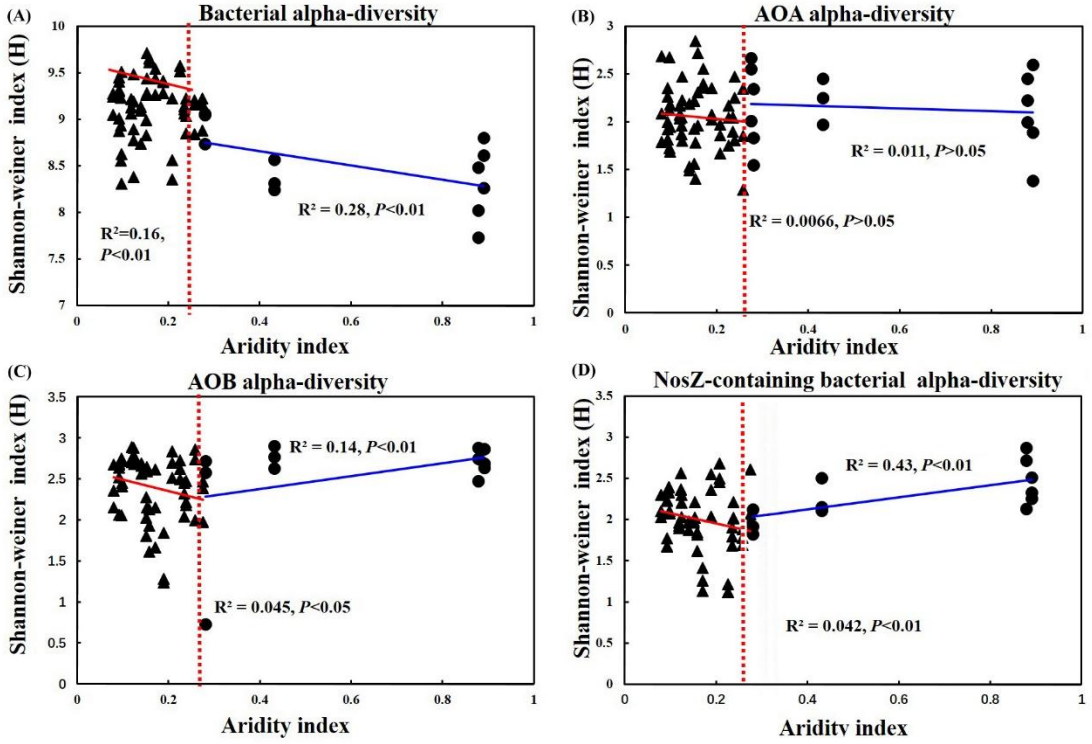
(A)
Bacterial alpha-diversity
Shannon-weiner index (H)
Aridity index
R²=0.16, P<0.01
R² = 0.28, P<0.01
(B)
AOA alpha-diversity
Shannon-weiner index (H)
Aridity index
R² = 0.011, P>0.05
R² = 0.0066, P>0.05
(C)
AOB alpha-diversity
Shannon-weiner index (H)
Aridity index
R² = 0.14, P<0.01
R² = 0.045, P<0.05
(D)
NosZ-containing bacterial alpha-diversity
Shannon-weiner index (H)
Aridity index
R² = 0.43, P<0.01
R² = 0.042, P<0.01

Figure 7

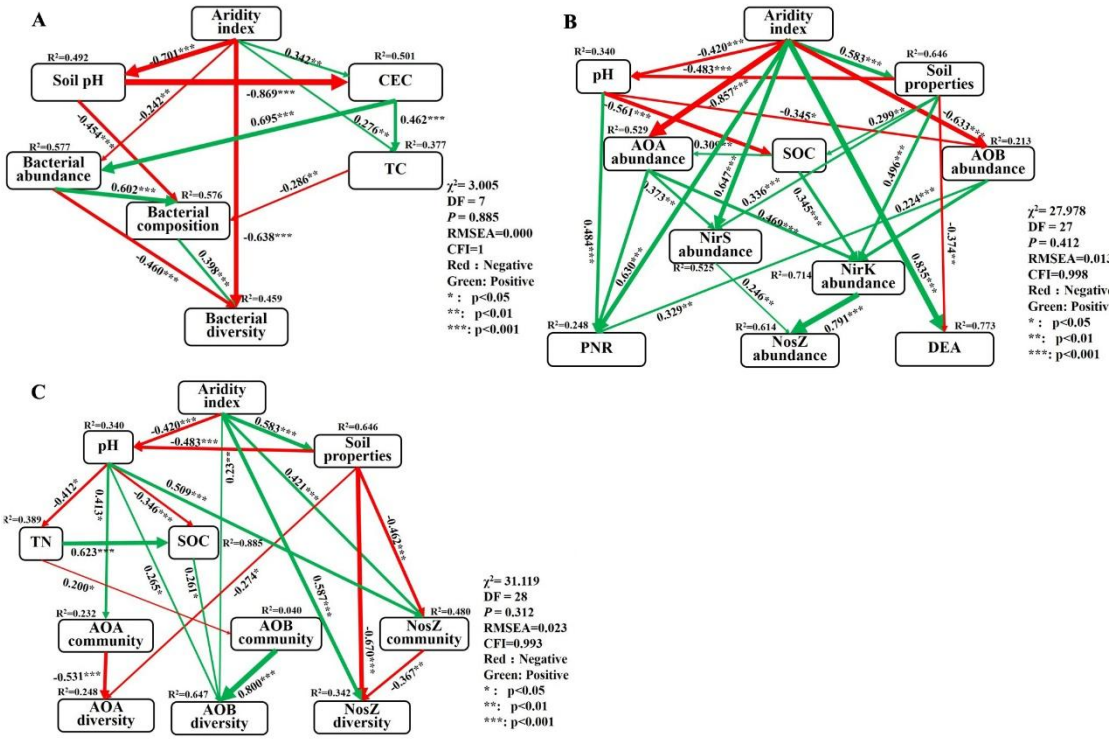
A
Aridity index
Soil pH
CEC
Bacterial abundance
TC
Bacterial composition
Bacterial diversity
χ²= 3.005
DF = 7
P = 0.885
RMSEA=0.000
CFI=1
Red : Negative
Green: Positive
*: p<0.05
**: p<0.01
***: p<0.001
B
Aridity index
pH
Soil properties
AOA abundance
SOC
AOB abundance
NirS abundance
NirK abundance
PNR
NosZ abundance
DEA
χ²= 27.978
DF = 27
P = 0.412
RMSEA=0.01
CFI=0.998
Red : Negativ
Green: Positiv
*: p<0.05
**: p<0.01
***: p<0.001
C
Aridity index
pH
Soil properties
TN
SOC
AOA community
AOB community
NosZ community
AOA diversity
AOB diversity
NosZ diversity
χ²= 31.119
DF = 28
P = 0.312
RMSEA=0.023
CFI=0.993
Red : Negative
Green: Positive
*: p<0.05
**: p<0.01
***: p<0.001

Table S1 Geographical coordinates and environmental conditions of the soil samples

Sample name	Latitude (N)	Longitude (E)	Elevation (m)	Dominated vegetation	Plant cover (%)	Soil Type	Soil parental material
LZ-01	29°36'21"90	94°36'23"06	4185	Grass.,			
LZ-02	29°36'21"00	94°36'22"63	4208	Cyperaceae.,	>95	Boggy meadow soil	Magmatite-granite
LZ-03	29°36'21"55	94°36'22"87	4188	Primula L.,		Felty soil	
LZ-04	29°36'47"80	94°38'54"80	4504	Armoise L.,	>95	(Brown soil)	
LZ-05	29°36'47"65	94°38'54"67	4506	Potentilla L.,			
LZ-06	29°36'47"31	94°38'55"59	4520	Cyperaceae.,	>95		
LZ-07	29°52'37"37	92°32'41"58	4187	Grass.,		Alpine shrubby	Silicarenite
LZ-08	29°52'37"68	92°32'41"90	4191	Cyperaceae.,	>90	meadow soil	
LZ-09	29°52'37"132	92°32'41"80	4184	Iridaeeae.,		(Brown soil)	
				Caragana.,			
MLS-01	29°49'23"74	92°21'52"70	4941			Alpine meadow soil	
MLS-02	29°49'23"56	92°21'52"86	4951		>85	(Dark brown soil)	
MLS-03	29°49'23"32	92°21'52"46	4949	Pedicularis L.,			
YBJ-01	30°10'31"22	90°35'25"18	4516	Saxifraga L.,	≈85		Granite
YBJ-02	30°10'29"80	90°35'27"15	4522	Artemisia L.,		Brown soil	
YBJ-03	30°10'29"11	90°35'27"57	4532	Potentilla L.,			
DX-01	30°31'50"17	91°18'10"36	4354	Carex invaoviae.,	≈80		
DX-02	30°31'48"15	91°18'09"15	4359	Festuca ovina.,		Dark brown soil	
DX-03	30°31'51"70	91°18'18"73	4370	Oxytropis spp.,			
NQ-01	31°17'09"23	91°48'20"98	4660	Stipa capillace.,	≈80		
NQ-02	31°17'07"34	91°48'21"25	4670				
NQ-03	31°17'06"66	91°48'19"50	4677			Dark brown soil	
NQ-04	31°38'46"42	92°00'47"16	4591				
NQ-05	31°38'45"16	92°00'43"29	4601		≈80		
NQ-06	31°38'46"30	92°00'50"90	4601				
					≈80		
					≈80		
NMC-01	30°48'07"40	91°06'29"90	4773	Stipa purpurea.,		Desert steppe soil	Psammite
NMC-02	30°48'07"90	91°06'29"70	4764	Kobresia	≈40	(Grey desert soil)	
NMC-03	30°48'09"71	91°06'32"08	4770	macrantha.,			

BG-01	31°17'30"07	90°20'25"72	4652				Granite
BG-02	31°17'30"30	90°20'30"17	4641				
BG-03	31°17'31.40	90°20'30.91	4646		70%		
BG-04	31°28'39.70	89°54'30.72	4755	Bunch grass.,			Sandstone
BG-05	31°28'42.35	89°54'28.29	4761	Kobresia L.,			
BG-06	31°28'41.04	89°54'25.13	4770	Poa crymophila.,		Alpine steppe soil	
BG-07	31°36'51.25	89°36'40.22	4598	Carex			
BG-08	31°36'51.72	89°36'39.65	4597	moorcroftii.,			
BG-09	31°36'52.22	89°36'41.18	4594	Orinus thoroldii.,			
NM-01	31°37'15.31	88°52'09.52	4645	Artemisia			Sandstone
NM-02	31°37'17.17	88°52'09.96	4637	wellbyi.,	60%		
NM-03	31°37'16.10	88°52'13.63	4642				
NM-04	31°51'13.52	87°46'04.83	4612				
NM-05	31°51'11.97	87°46'03.64	4596				
NM-06	31°51'10.85	87°46'04.62	4597				
NM-07	31°54'11.82	86°16'39.54	4768				
NM-08	31°54'11.81	86°16'37.51	4767				
NM-09	31°54'12.21	86°16'35.63	4767				
GZ-01	32°12'56.81	84°29'57.58	4473				Sandstone
GZ-02	32°12'55.56	84°29'58.07	4473				
GZ-03	32°12'53.33	84°29'55.90	4476				
GZ-04	32°17'17.01	84°06'57.76	4437		≈30		
GZ-05	32°17'14.75	84°06'57.38	4452				
GZ-06	32°17'12.99	84°06'59.10	4446				
CQ-01	32°18'41.20	85°07'26.26	4723				
CQ-02	32°18'39.36	85°07'26.94	4714	Kobresia L.,			Sandstone
CQ-03	32°18'39.93	85°07'26.97	4719	Stipa capillace.,			
CQ-04	30°50'22.01	85°05'59.76	4729	Oxytropis spp.,		Alpine desert soil	
CQ-05	30°50'21.16	85°05'59.84	4724	Poa crymophila.,		(Grey desert soil)	
CQ-06	30°50'20.60	85°06'00.67	4725		≈20		
CQ-07	30°34'55.82	85°24'03.21	4805				
CQ-08	30°34'55.03	85°24'04.81	4809				
CQ-09	30°34'52.22	85°24'04.14	4804				
CQ-10	30°09'30.95	85°22'56.46	5373				
CQ-11	30°09'31.11	85°22'55.57	5373		≈10		
CQ-12	30°09'31.33	85°22'56.62	5378				

SG-01	29°05'17.62	85°23'23.42	4696	Kobresia L.,			Shale
SG-02	29°05'17.59	85°23'22.98	4701	Pennisetum L.,	≈30		
SG-03	29°05'17.24	85°23'21.45	4714	Polygonum L.,			
DR-01	28°51'06.91	87°20'13.32	4908	Oxytropis L.,		Alpine steppe soil	Shale
DR-02	28°51'06.76	8^{7o}20'14.47	4915	Tribulus L.,		(Yellow brown soil)	
DR-03	28°51'07.07	87°20'14.92	4922		≈40		
RKZ-01	29°19'49.48	89°10'52.79	3827				Psammite
RKZ-02	29°19'48.95	89°10'53.13	3835				
RKZ-03	29°19'49.05	89°10'53.72	3839				
					≈50		

Abbrev Letter and number mean sampling locations: LZ: Nyingchi; MLS: Mila Mountain; YBJ: Yambajan; DX: Damxung; NQ: Nagchu; NMC: Namco; BG: Bangor; NM: Nima; GZ: Gerze; CQ: Cuoqin; SG: Saga; DR: Tingri; RKZ: Shigatse.

Table S2 List of PCR primers used in this study for T-RFLP and sequencing analyses

Target gene	Primer set	Sequences (5'-3')	qPCR efficiency	Thermal profile	References
16S rRNA	27F	AGAGTTTGATCCTGGCTCAG		**qPCR:** 95℃/10 s; 40 cycles of 95℃/15 s, 56℃/1 min	Lane, 1991
	1492R	TACGGCTACCTTGTTACGACTT			
Probe	1369 F[a]	CGGTGAATACGTTCYCGG		**Clone library:** 94℃/5 min; 30 cycles of 94℃/30 s, 54℃/30 s, 72 ℃/1 min, 72℃/10 min	
	TM1389F[a]	CTTGTACACACCGCCCGTC			Suzuki *et al*., 2000
amoA (AOA)	CrenamoA23f[b]	ATGGTCTGGCTWAGACG	87%	**qPCR:** 95℃/1 min; 35 cycles of 95℃/30 s, 55℃/30 s,72℃/30 s. **Clone library:** 94℃/5 min; 10 cycles of 94℃/30 s, 60℃/30 s (-0.5℃/cycle), 72 ℃/30 s; 25 cycles of 94℃/30 s, 55℃/45 s, 72 ℃/1 min, 72℃/5 min.	Avrahami *et al*., 2003
	CrenamoA616r	GCCATCCATCTGTATGTCCA			
amoA (AOB)	amoA1F[b]	GGGGTTTCTACTGGTGGT	85%	**qPCR:** 95℃/1 min; 35 cycles of 95℃/30 s, 60℃/30 s,72℃/30 s. **Clone library:** 94℃/5 min; 10 cycles of 94℃/30 s, 62℃/45 s (-0.5℃/cycle), 72 ℃/1 min; 25 cycles of 94℃/30 s, 57℃/45 s, 72 ℃/1 min, 72℃/5 min.	Rotthauwe *et al*., 1997
	amoA2R	CCCCTCKGSAAAGCCTTCTTC			
nirS	Nirs-cd3aF[b]	GTSAACGTSAAGGARACSGG	97%	**qPCR:** 94℃/2 min; 5 cycles of 94℃/1 min, 58℃/1 min (-1℃/cycle), 72℃/30 s; 30 cycles of 94℃/30 s, 53℃/1 min, 72 ℃/30 s. **Clone library:** 95℃/5 min; 6 cycles of 95℃/15 s, 63℃/30 s (-1 ℃/cycle), 72 ℃/30 s; 25 cycles of 95℃/15 s, 58℃/30 s, 72 ℃/30 s, 72℃/5 min.	Michotey *et al*., 2000 Throback *et al*., 2004
	Nirs-R3cd	GASTTCGGRTGSGTCTTGA			
nirK	nirK-F1aCu[b]	ATCATGGTSCTGCCGCG	95%	**qPCR:** 95℃/3 min; 6 cycles of 95℃/30 s, 63℃/30 s (-1℃/cycle), 72 ℃/30 s; 30 cycles of 95℃/30	Throback *et al*., 2004
	nirK-R3Cu	GCCTCGATCAGRTT			

		GTGGTT		s, 58℃/30 s, 72℃/30 s. **Clone library:** 95℃/5 min; 6 cycles of 95℃/30 s, 63℃/30 s (-1 ℃/cycle), 72 ℃/20 s; 25 cycles of 95℃/30 s, 58℃/30 s, 72 ℃/30 s, 72℃/5 min.	
nosZ	nosZF[b]	CGYTGTTCMTCGACAGCCAG	97%	**qPCR:** 95℃/1 min; 6 cycles of 95℃/30 s, 65℃/30 s (-1℃/cycle), 72 ℃/30 s; 30 cycles of 95℃/30 s, 60℃/30 s, 72℃/30 s. **Clone library:** 95℃/5 min; 30 cycles of 95℃/30 s, 60℃/30 s, 72 ℃/30 s, 72℃/5 min.	Henry *et al*., 2006
	nosZ2R[c]	CAKRTGCAKSGCRTGGCAGAA			
	nosZ2F	CGCRACGGCAASAAGGTSMSSGT			

[a] Bacterial probe sequences. [b](6-FAM) was attached to the 5' end of the primers. [c] **(**nosZ-F+nosZ2R) were used for *nosZ* gene T-RFLP analysis.

Table S3. Spearman correlation between soil physical and chemical properties and microbial community gene abundances and enzyme activity

Soil parameters	*Bacteria*	AOA	AOB	*NirS*	*NirK*	*NosZ*	PNR	DEA
Aridity index	**0.48****	-0.16	-0.13	**0.38****	**0.52****	**0.55****	-0.66	**0.51****
Longitude	**0.42****	-0.12	0.058	**0.43****	**0.30****	**0.53****	0.0040	**0.53****
Latitude	**-0.29***	0.13	0.061	**-0.28***	**-0.61****	**-0.39****	-0.035	-0.21
Elevation (m)	0.037	**0.29***	**0.39****	0.059	-0.0030	0.18	**0.24***	-0.11
MAP (mm)	**0.38****	-0.18	-0.12	**0.37****	**0.46****	**0.52****	-0.11	**0.51****
MAT (^{o}C)	-0.025	**-0.43****	**-0.35****	-0.13	**0.27***	-0.12	-0.21	0.14
CEC (cmol kg^{-1})	**0.72****	0.20	0.066	**0.53****	**0.60****	**0.66****	0.20	**0.55****
Clay (%)	0.19	-0.19	-0.072	0.13	**0.43****	**0.39****	-0.72	**0.29***
Sandy (%)	-0.097	0.20	0.12	-0.082	**-0.43****	**-0.33****	0.079	**-0.29***
pH	**-0.46****	0.0090	0.10	**-0.43****	**-0.55****	**-0.77****	0.016	**-0.76****
SMC (%)	**0.61****	0.022	-0.074	**0.40****	**0.62****	**0.58****	0.12	**0.59****
TN (%)	**0.71****	**0.25****	0.20	**0.63****	**0.53****	**0.67****	**0.32****	**0.52****
TC (%)	**0.63****	0.14	0.10	**0.37****	**0.44****	**0.45****	**0.32****	**0.38****
SOC (g kg^{-1})	**0.68****	**0.25***	0.0070	**0.50****	**0.67****	**0.70****	**0.25***	**0.64****
NH_4^+ (g·kg^{-1})	**0.37****	0.060	0.043	0.14	**0.32****	**0.23***	0.22	**0.38****
NO_3^- (g kg^{-1})	**0.25***	**-0.27***	-0.23	**0.28***	0.15	**0.36****	**-0.37****	**0.48****
C/N	**0.46****	0.12	**-0.25***	**0.23***	**0.60****	**0.55****	-0.31	**0.60****

MAP: mean annul pricipitation; MAT: mean annul temperature; SMC: soil moisture content; TN: soil total nitrogen; TC: soil total carbion; SOC: soil organic carbon; C/N: the ratio of SOC to TN.

Table S4. Mantel correlations between the microbial community structure and soil characteristics

Soil parameters	*Bacteria*	AOA	AOB	*NosZ*
Longitude	**0.48****	**0.32****	**0.22****	**0.09***
Latitude	**0.19****	**0.10****	**0.06***	**0.13****
Elevation	**0.21****	**0.06**	0.022	0.009
MAP (mm)	**0.65****	**0.32****	**0.21****	**0.26****
MAT(^{o}C)	**0.26****	**0.20****	0.014	0.077
Aridity index	**0.69****	**0.30****	**0.20****	**0.10***
pH	**0.47****	**0.25****	**0.164****	**0.22****
SMC (%)	**0.57****	**0.22****	**0.26****	**0.18****
CEC	**0.28****	**0.17****	**0.23****	**0.13***
TN (%)	**0.35****	**0.18****	**0.16****	0.10
TC (%)	**0.29****	**0.12***	0.07	0.046
SOC	**0.42****	**0.24****	**0.26****	**0.18****
NH_4^+	**0.38****	**0.15****	**0.20****	0.036
NO_3^-	**0.30****	**0.24****	**0.25****	**0.091***

MAP: mean annul pricipitation; MAT: mean annul temperature; SMC: soil moisture content; TN: soil total nitrogen; TC: soil total carbion; SOC: soil organic carbon; C/N: the ratio of SOC to TN.

Supplementary figure legends

Figure S1 The shift of AOA community compositions along the aridity gradient.

Figure S2 Neighbor-joining phylogenetic tree based on archaeal *amoA* gene clone library from alpine grassland soils of the Tibetan Plateau, numbers on the nodes are the bootstrap values (percentages) based on 1,000 replicates and values of above 50% were presented. The sequences identified for the TRFs digested by the *Rsa* I enzyme.

Figure S3 The shift of AOB community compositions along the aridity gradient.

Figure S4 Neighbor-joining phylogenetic tree based on bacterial *amoA* gene clone library from alpine grassland soils of the Tibetan Plateau, numbers on the nodes are the bootstrap values (percentages) based on 1,000 replicates and values of above 50% were presented. The sequences identified for the TRFs digested by the *Hha* I enzyme.

Figure S5 The shift of *nosZ*-containing bacterial community compositions along the aridity gradient.

Figure S6 Neighbor-joining phylogenetic tree based on *nosZ*-containing bacterial clone library from alpine grassland soils of the Tibetan Plateau, numbers on the nodes are the bootstrap values (percentages) based on 1,000 replicates and values of above 50% were presented. The sequences identified for the TRFs digested by the *Hae* III enzyme.

Figure S7 (A) Standardized total effects of AI (direct plus indirect effects) on bacterial abundance, composition and diversity; (B) Standardized total effects of AI on N cycling functional gene abundances and N turnover enzyme activities; (C)

Standardized total effects of AI on composition and diversity of bacteria, ammonia-oxidizers and denitrifer.

Figure S1

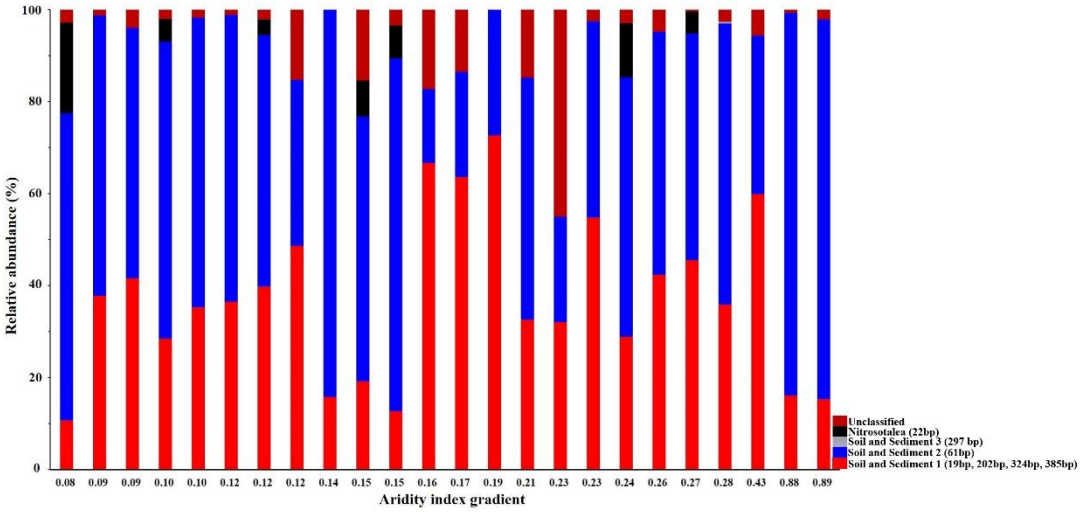
Relative abundance (%)
100
80
60
40
20
0
0.08 0.09 0.09 0.10 0.10 0.12 0.12 0.12 0.14 0.15 0.15 0.16 0.17 0.19 0.21 0.23 0.23 0.24 0.26 0.27 0.28 0.43 0.88 0.89
Aridity index gradient
Unclassified
Nitrosotalea (22bp)
Soil and Sediment 3 (297 bp)
Soil and Sediment 2 (61bp)
Soil and Sediment 1 (19bp, 202bp, 324bp, 385bp)

Figure S2

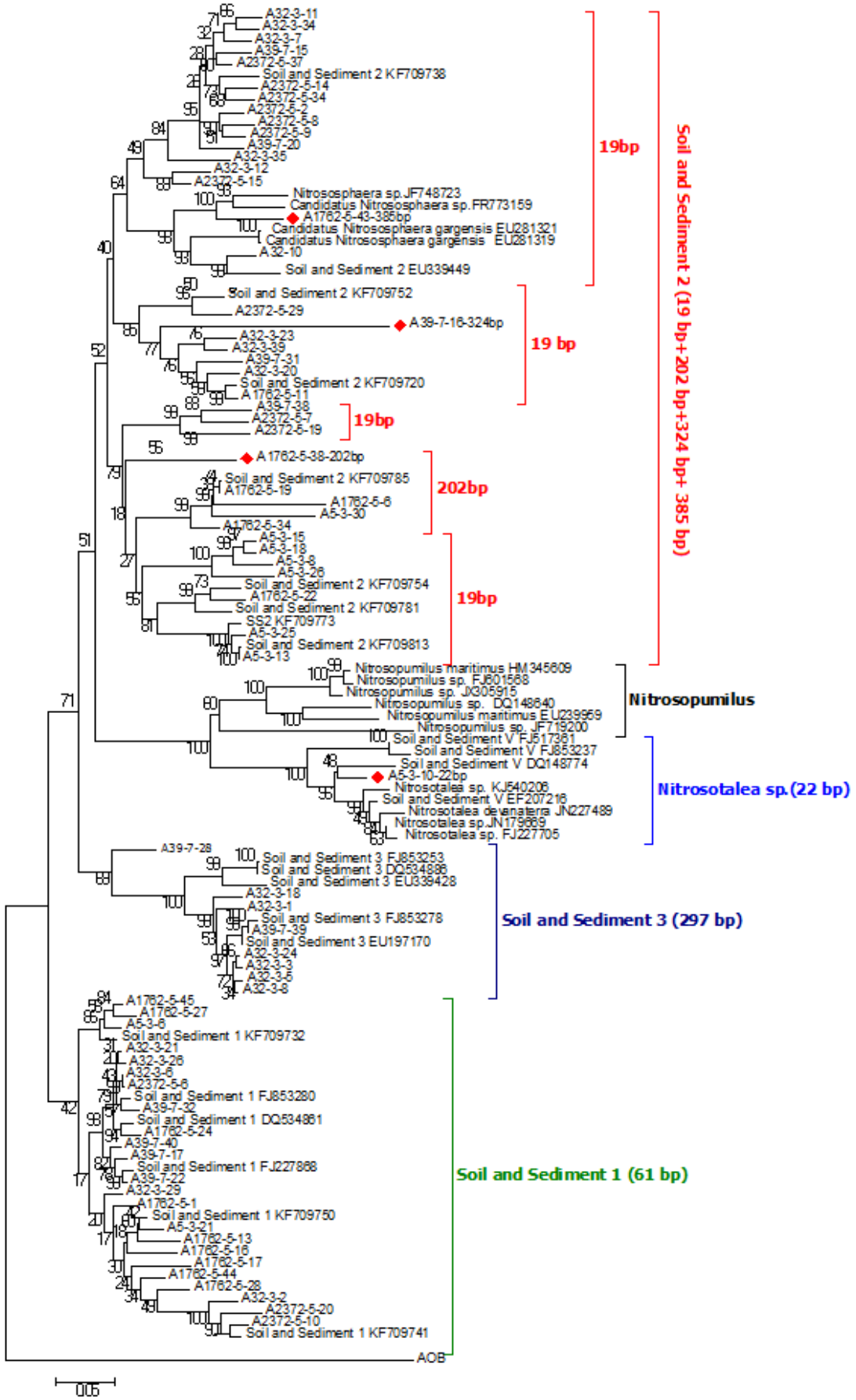
A32-3-11
A32-3-34
A32-3-7
A39-7-15
A2372-5-37
Soil and Sediment 2 KF709738
A2372-5-14
A2372-5-34
A2372-5-2
A2372-5-8
A2372-5-9
A39-7-20
A32-3-35
A32-3-12
A2372-5-15
Nitrososphaera sp.JF748723
Candidatus Nitrososphaera sp.FR773159
A1762-5-43-385bp
Candidatus Nitrososphaera gargensis EU281321
Candidatus Nitrososphaera gargensis EU281319
A32-10
Soil and Sediment 2 EU339449
Soil and Sediment 2 KF709752
A2372-5-29
A39-7-16-324bp
A32-3-23
A32-3-39
A39-7-31
A32-3-20
Soil and Sediment 2 KF709720
A1762-5-11
A39-7-38
A2372-5-7
A2372-5-19
A1762-5-38-202bp
Soil and Sediment 2 KF709785
A1762-5-19
A1762-5-6
A5-3-30
A1762-5-34
A5-3-15
A5-3-18
A5-3-8
A5-3-26
Soil and Sediment 2 KF709754
A1762-5-22
Soil and Sediment 2 KF709781
SS2 KF709773
A5-3-25
Soil and Sediment 2 KF709813
A5-3-13
Nitrosopumilus maritimus HM345609
Nitrosopumilus sp. FJ601568
Nitrosopumilus sp. JX305915
Nitrosopumilus sp. DQ148640
Nitrosopumilus maritimus EU239959
Nitrosopumilus sp. JF719200
Soil and Sediment V FJ517361
Soil and Sediment V FJ853237
Soil and Sediment V DQ148774
A5-3-10-22bp
Nitrosotalea sp. KJ540206
Soil and Sediment V EF207216
Nitrosotalea devanaterra JN227489
Nitrosotalea sp.JN179669
Nitrosotalea sp. FJ227705
A39-7-28
Soil and Sediment 3 FJ853253
Soil and Sediment 3 DQ534886
Soil and Sediment 3 EU339428
A32-3-18
A32-3-1
Soil and Sediment 3 FJ853278
A39-7-39
Soil and Sediment 3 EU197170
A32-3-24
A32-3-3
A32-3-5
A32-3-8
A1762-5-45
A1762-5-27
A5-3-6
Soil and Sediment 1 KF709732
A32-3-21
A32-3-26
A32-3-6
A2372-5-6
Soil and Sediment 1 FJ853280
A39-7-32
Soil and Sediment 1 DQ534881
A1762-5-24
A39-7-40
A39-7-17
Soil and Sediment 1 FJ227868
A39-7-22
A32-3-29
A1762-5-1
Soil and Sediment 1 KF709750
A5-3-21
A1762-5-13
A1762-5-16
A1762-5-17
A1762-5-44
A1762-5-28
A32-3-2
A2372-5-20
A2372-5-10
Soil and Sediment 1 KF709741
AOB
0.05
19bp
19 bp
19bp
202bp
19bp
Soil and Sediment 2 (19 bp+202 bp+324 bp+ 385 bp)
Nitrosopumilus
Nitrosotalea sp.(22 bp)
Soil and Sediment 3 (297 bp)
Soil and Sediment 1 (61 bp)

Figure S3

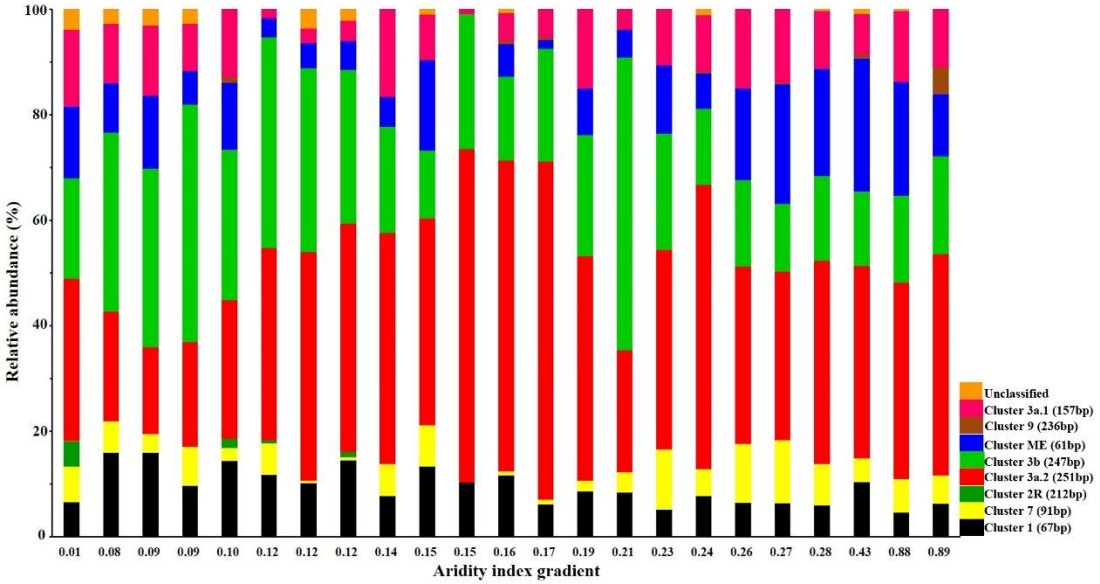
Relative abundance (%)
100
80
60
40
20
0
0.01
0.08
0.09
0.09
0.10
0.12
0.12
0.12
0.14
0.15
0.15
0.16
0.17
0.19
0.21
0.23
0.24
0.26
0.27
0.28
0.43
0.88
0.89
Aridity index gradient
Unclassified
Cluster 3a.1 (157bp)
Cluster 9 (236bp)
Cluster ME (61bp)
Cluster 3b (247bp)
Cluster 3a.2 (251bp)
Cluster 2R (212bp)
Cluster 7 (91bp)
Cluster 1 (67bp)

Figure S4

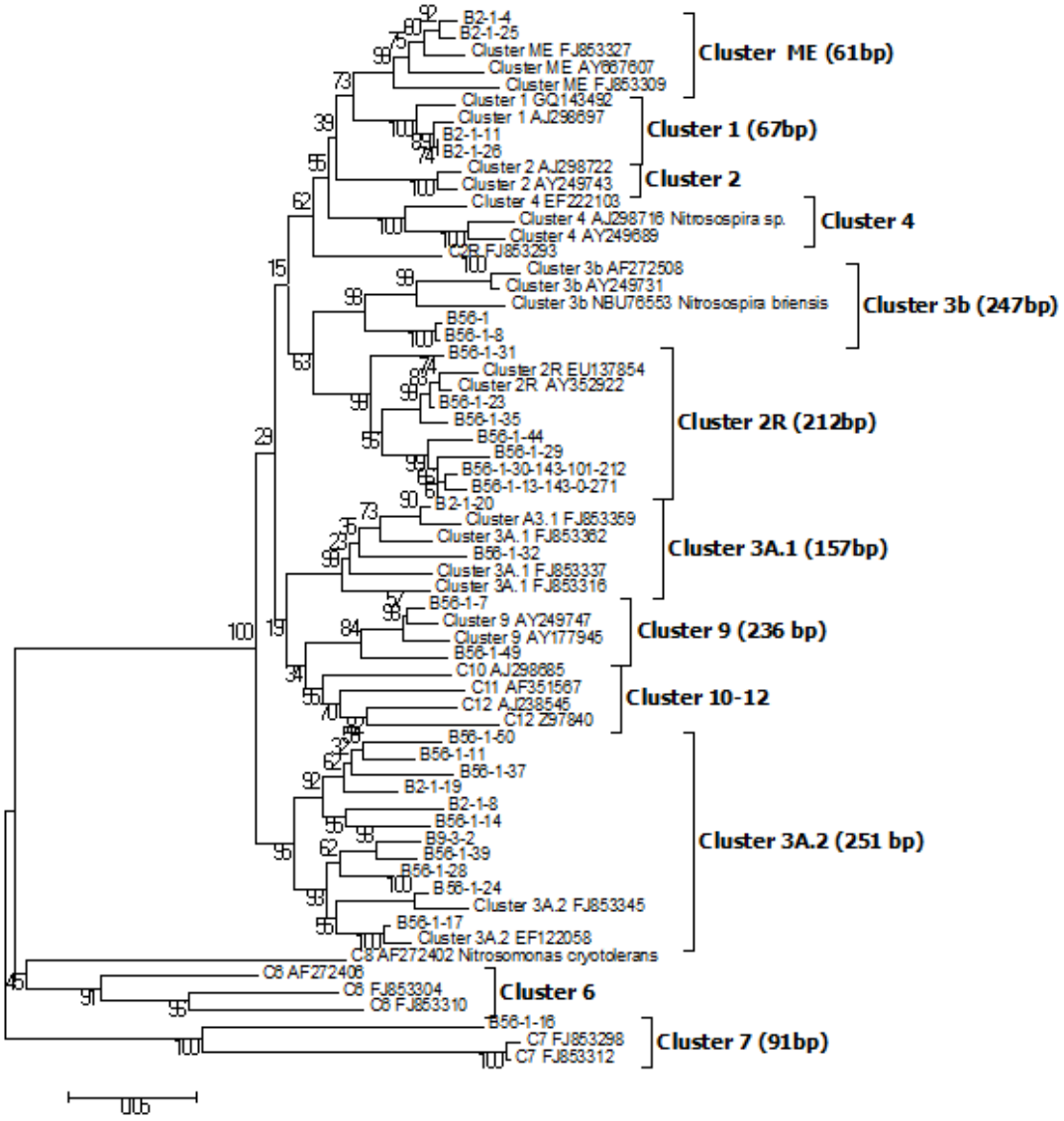
B2-1-4
B2-1-25
Cluster ME FJ853327
Cluster ME AY667607
Cluster ME FJ853309
Cluster ME (61bp)
Cluster 1 GQ143492
Cluster 1 AJ298697
B2-1-11
B2-1-26
Cluster 1 (67bp)
Cluster 2 AJ298722
Cluster 2 AY249743
Cluster 2
Cluster 4 EF222103
Cluster 4 AJ298716 Nitrosospira sp.
Cluster 4 AY249689
Cluster 4
C2R FJ853293
Cluster 3b AF272508
Cluster 3b AY249731
Cluster 3b NBU76553 Nitrosospira briensis
Cluster 3b (247bp)
B56-1
B56-1-8
B56-1-31
Cluster 2R EU137854
Cluster 2R AY352922
B56-1-23
B56-1-35
B56-1-44
B56-1-29
B56-1-30-143-101-212
B56-1-13-143-0-271
Cluster 2R (212bp)
B2-1-20
Cluster A3.1 FJ853359
Cluster 3A.1 FJ853362
B56-1-32
Cluster 3A.1 FJ853337
Cluster 3A.1 FJ853316
Cluster 3A.1 (157bp)
B56-1-7
Cluster 9 AY249747
Cluster 9 AY177945
B56-1-49
Cluster 9 (236 bp)
C10 AJ298885
C11 AF351567
C12 AJ238545
C12 Z97840
Cluster 10-12
B56-1-50
B56-1-11
B56-1-37
B2-1-19
B2-1-8
B56-1-14
B9-3-2
B56-1-39
B56-1-28
B56-1-24
Cluster 3A.2 FJ853345
B56-1-17
Cluster 3A.2 EF122058
Cluster 3A.2 (251 bp)
C8 AF272402 Nitrosomonas cryotolerans
C8 AF272406
C8 FJ853304
C8 FJ853310
Cluster 6
B56-1-16
C7 FJ853298
C7 FJ853312
Cluster 7 (91bp)
0.05

Figure S5

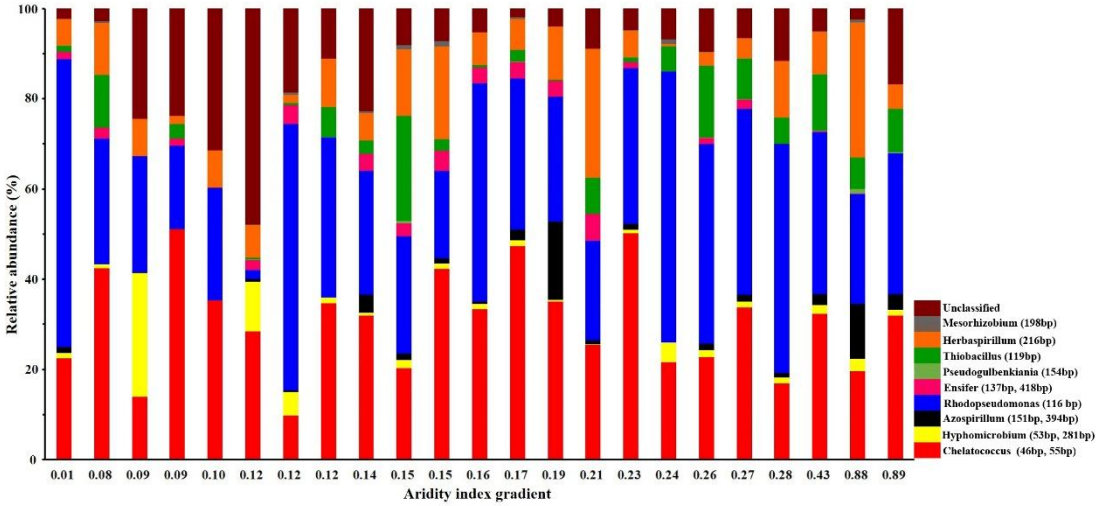
Relative abundance (%)
100
80
60
40
20
0
0.01
0.08
0.09
0.09
0.10
0.12
0.12
0.12
0.14
0.15
0.15
0.16
0.17
0.19
0.21
0.23
0.24
0.26
0.27
0.28
0.43
0.88
0.89
Aridity index gradient
Unclassified
Mesorhizobium (198bp)
Herbaspirillum (216bp)
Thiobacillus (119bp)
Pseudogulbenkiania (154bp)
Ensifer (137bp, 418bp)
Rhodopseudomonas (116 bp)
Azospirillum (151bp, 394bp)
Hyphomicrobium (53bp, 281bp)
Chelatococcus (46bp, 55bp)

Figure S6

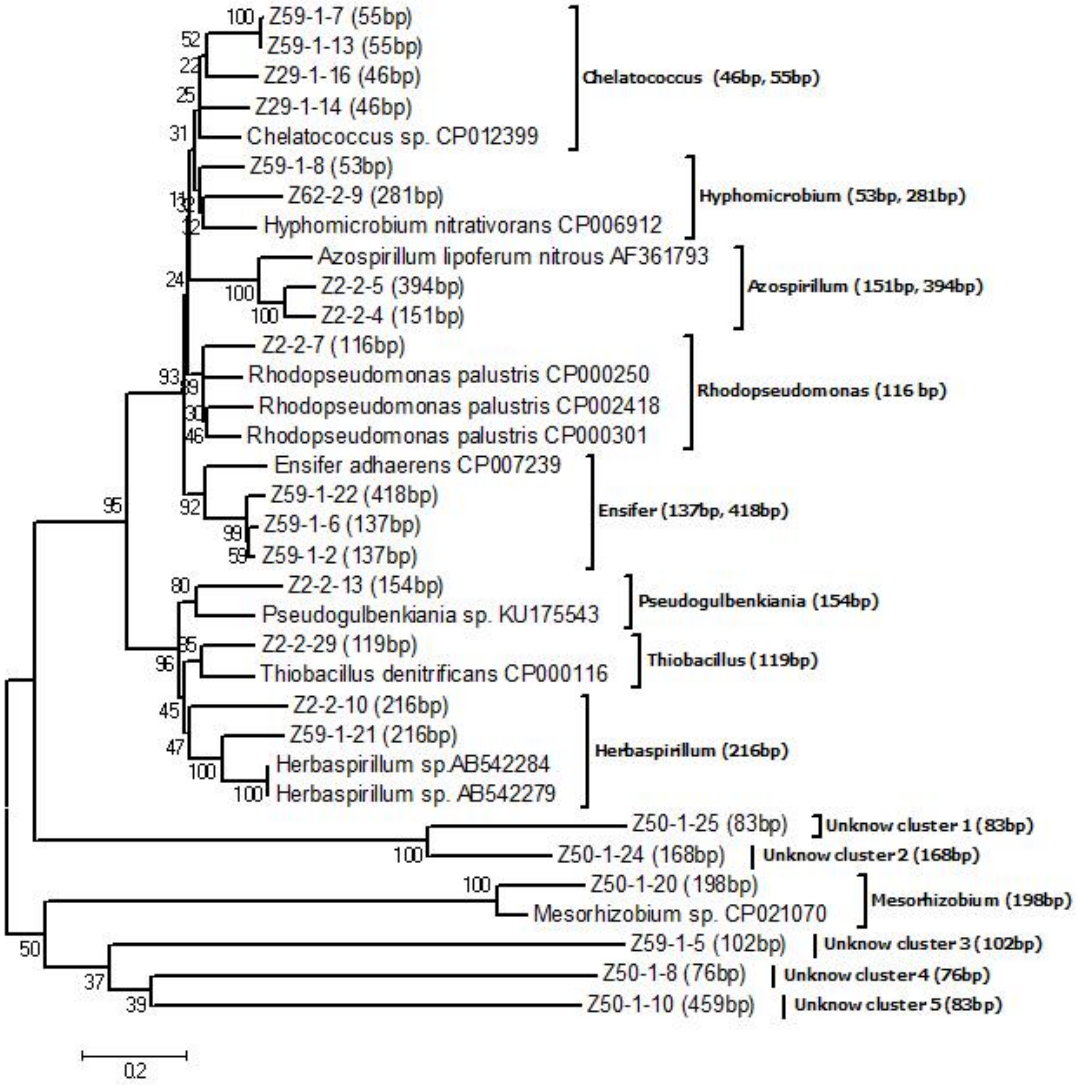
Z59-1-7 (55bp)
Z59-1-13 (55bp)
Z29-1-16 (46bp)
Z29-1-14 (46bp)
Chelatococcus sp. CP012399
Chelatococcus (46bp, 55bp)
Z59-1-8 (53bp)
Z62-2-9 (281bp)
Hyphomicrobium nitrativorans CP006912
Hyphomicrobium (53bp, 281bp)
Azospirillum lipoferum nitrous AF361793
Z2-2-5 (394bp)
Z2-2-4 (151bp)
Azospirillum (151bp, 394bp)
Z2-2-7 (116bp)
Rhodopseudomonas palustris CP000250
Rhodopseudomonas palustris CP002418
Rhodopseudomonas palustris CP000301
Rhodopseudomonas (116 bp)
Ensifer adhaerens CP007239
Z59-1-22 (418bp)
Z59-1-6 (137bp)
Z59-1-2 (137bp)
Ensifer (137bp, 418bp)
Z2-2-13 (154bp)
Pseudogulbenkiania sp. KU175543
Pseudogulbenkiania (154bp)
Z2-2-29 (119bp)
Thiobacillus denitrificans CP000116
Thiobacillus (119bp)
Z2-2-10 (216bp)
Z59-1-21 (216bp)
Herbaspirillum sp.AB542284
Herbaspirillum sp. AB542279
Herbaspirillum (216bp)
Z50-1-25 (83bp)
Unknow cluster 1 (83bp)
Z50-1-24 (168bp)
Unknow cluster 2 (168bp)
Z50-1-20 (198bp)
Mesorhizobium sp. CP021070
Mesorhizobium (198bp)
Z59-1-5 (102bp)
Unknow cluster 3 (102bp)
Z50-1-8 (76bp)
Unknow cluster 4 (76bp)
Z50-1-10 (459bp)
Unknow cluster 5 (83bp)
0.2

Figure S7

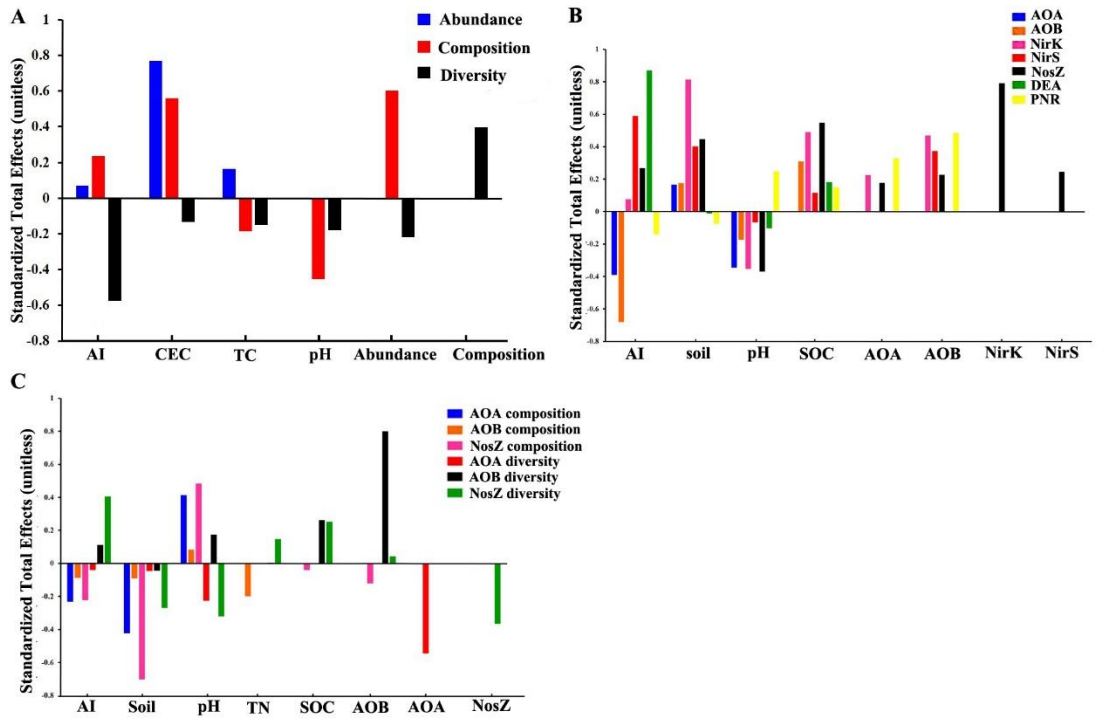
A
Abundance
Composition
Diversity
Standardized Total Effects (unitless)
AI
CEC
TC
pH
Abundance
Composition
B
AOA
AOB
NirK
NirS
NosZ
DEA
PNR
Standardized Total Effects (unitless)
AI
soil
pH
SOC
AOA
AOB
NirK
NirS
C
AOA composition
AOB composition
NosZ composition
AOA diversity
AOB diversity
NosZ diversity
Standardized Total Effects (unitless)
AI
Soil
pH
TN
SOC
AOB
AOA
NosZ